SHARING

SELF-ORGANIZED HETEROGENEOUS ADVANCED RADIO NETWORKS GENERATION

Deliverable D4.5

Spectrum allocation: innovative concepts and performance evaluation

Date of delivery	09/03/2015
Contractual date of delivery	31/01/2015
Project number	C2012/1-8
Editor(s)	Mourad KHANFOUCI (MERCE)
Author(s)	Mourad KHANFOUCI (MERCE), Nicolas GRESSET (MERCE), Mehdi Bennis (UOULU), Mohamad Assaad (SUPELEC),
Dissemination level	PU
Workpackage	4
Version	V0.1
Total number of pages	37

Abstract:

This deliverable provides an updated view on innovative concepts on spectrum allocation for heterogeneous network deployments. In addition to the concept description, this deliverable will present some results and performance assessments for advanced carrier aggregation, radio resource allocation mechanisms and distributed synchronization for typical heterogeneous network (HetNet) deployments.

This deliverable will also discuss the performance of spectrum use and resource allocations strategies for heterogeneous networks for different deployment scenarios.

Keywords:

Performance, Heterogeneous Networks, RRM, SON, Spectrum, Management, Algorithm

Document Revision History

Version	Date	Author	Summary of main changes
0.1	29/09/2014	Mourad KHANFOUCI	Initial TOC

TABLE OF CONTENTS

EXECUTIVE SUMMARY

SHARING Work Package 4 Task 4.4 studies various self-organizing techniques for radio resource allocation, taking into account carrier aggregation features within heterogeneous network (HetNet) deployments. For example, distributed and centralized radio resource management strategies are considered for ensuring the stability of the network while improving its energy efficiency. Furthermore, a learning framework is proposed for improving performance of RRM strategies and interference management mechanisms based on dynamic carrier selection in LTE-A systems with carrier aggregation capabilities.

The proposed mechanisms are SON- flavored algorithms for the selection of primary and secondary component carriers for a group of base stations randomly deployed in campus scenario with the goal of improving the throughput of the conventional coordinated multi-point schemes .The component carrier selection is based on UE measurements and statistical information about the usage of the component carriers and is based on graph coloring techniques. Furthermore, the topic of dynamic component carrier selection will be discussed in the context of multi-flow carrier aggregation, where user terminals aggregate separate flows coming from different nodes. This multi-flow carrier aggregation will be enhanced with learning mechanisms. Finally, since tight time synchronization is required, task 4.4 propose and develop a cooperative distributed synchronization mechanism, which improves the basic time reference provided by the macro network, based on leader-follower consensus averaging techniques.

1 INTRODUCTION

Traffic in the mobile networks is expected to grow very rapidly in the coming years [Cis14][Eri13]. This traffic growth will be caused both by the evolution of mobile terminals (an increasing penetration of smartphones, tablets and mobile computers) and the increased use of more traffic-heavy services, especially video. It is also expected that the wider introduction of various cloud-based services and machine-to-machine communication will accelerate the traffic growth even further.

In general, there are three possible ways to increase the capacity of a mobile network: increased spectrum, improved spectral efficiency and network densification.

From the spectrum point of view, the capacity can be enhanced by deploying additional carriers, or by increasing the carrier bandwidth. The spectral efficiency can be improved both by improving the signal-to-interference-ratio for the link between the transmitter and the receiver and by introducing new techniques to enhance the utilization of the high signal-to-interference-ratio conditions. These techniques include for example advanced multi-antenna techniques (for example MIMO and beamforming), higher order modulations and advanced interference management (for example interference cancellation, inter-cell interference coordination and coordinated multipoint transmission and reception). However, although the achievable capacity gains via additional spectrum, and improvements in spectral efficiency are considerable, the substantial growth that is predicted for the mobile broadband revolution will require also actions to densify the mobile networks, i.e. to increase the *spatial reuse* of the radio resources.

This deliverable presents updates from the studies, initially presented in [D4.1] regarding:

- Carrier aggregation techniques that optimize the resource usage and the quality of service (QoS) of the system.
- Distributed radio resource management techniques that are robust to traffic parameter uncertainities
- Long term, low overhead radio resource management techniques that improves the average performance of the system outage SINR
- Consensus based synchronization technique that have the objective to correct in a decentralized manner clock drifts of large groups of randomly deployed base stations.

All these techniques are considered in the context of random deployment of the pico/femto base stations with additional uncertainities regarding traffic parameters and constraints concerning inter pico/femto signaling and spectrum resource usage..

The distributed synchronization technique presented in section 2.2.3 is a key enabler to the challenging carrier aggregation studies since it is capable to allow good timing reference and to correct clock drifts for large group of femto base stations deployed in the neighborhood of the macro network layer, so leading into further developpement of the decentralization of the proposed techniques. The plan of the deliverable is given by the following: in section 2.1carrier aggregation techniques for heterogeneous networks are presented. In section 2.1.1 a technique based on graph coloring is evaluated for the throughput optimization of combined Coordinated Multipoint transmission (CoMP) with Carrier Aggregation (CA). In section 2.1.2 multi- flow carrier aggregation concept is presented and initial performance evaluation is shown. Section 2.2 of the deliverable is devoted to the presentation of the innovations related to distributed Radio Ressources management RRM and distributed synchronization techniques. In section2.2.1, distributed downlink power control solution is presented for communication networks having unpredictable traffic arrival and mobility patterns. Section 2.2.2 presents some ideas and evaluations for distributed downlink power control with no information exchange between the transmitters. Finaly, the section 2.2.3 present some ideas regarding distributed synchronization techniques based on leader/follower consensus averaging techniques with errors in the consensus feedback.

2 SPECTRUM RESOURCE ALLOCATION MECHANISMS

One of the important aspects in future network deployment will be the increasing bandwidth demand, which is in confrontation with spectrum availability. In case of LTE-A networks, Carrier Aggregation (CA) will play an increasingly important role in providing operators the maximum flexibility for using their available spectrum. With CA, LTE-A will be able to deliver much higher throughputs than otherwise possible, by combining spectrum blocks up to 640MHz.

The scope of SHARING Task 4.4 is to study various self-organizing techniques for resource allocation, taking into account carrier aggregation features and capabilities of the future networks in the context of heterogeneous networks deployment. For example, the task will develop distributed and centralized radio resource management (RRM) strategies that ensure the stability of the network in the context of bursty traffic. Furthermore, the task will develop a learning framework in order to improve the performance of RRM strategies. A fundamental question that task 4.4 answers is how UEs can learn network parameters in order to improve their network utilities (rate, QoS, QoE, probability of success, etc). The task will also investigate an interference management mechanism based on dynamic carrier selection in LTE-A systems with carrier aggregation. This interference management is provided by SON-flavoured algorithms for the selection of primary and secondary component carriers for a group of base stations. The component carrier selection will be based on UE measurements and statistical information about the usage of the component carriers.

Furthermore, the topic of dynamic component carrier selection will be discussed in the context of multi-flow carrier aggregation, where UEs aggregate separate flows coming from different nodes. The proposed flexible assignment of primary and secondary component carriers is based on an original combination of cell range expansion and Q- learning techniques performed at the base stations.

Tight time synchronization is necessary for performing advanced RRM. Therefore, the task will propose a cooperative distributed synchronization mechanism, which will improve the basic time reference provided by the macro network.

2.1 Carrier aggregation

2.1.1 Coordinated carrier aggregation in campus of home base stations

In this work we introduce and describe Coordinated Carrier Aggregation (CCA) technique that is used for the resources usage optimization in a group of randomly deployed home base stations (HeNBs) performing joint radio resource management (JRRM) through coordination Gateway (GW). .

The proposed CCA scheme is improving the throughput of carrier aggregation capable UEs by the means of coordinated multi-point transmission (CoMP).

The carrier aggregation capable UE is receiving in this case data and/or control from multiple base stations that coordinate their transmission such *as not to use the same resources* for the transmission to the UE . This will ensure transparent operation for the UE and reduce the interference arising from CoMP transmission.

Description of the proposed coordinated carrier aggregation technique is given by the Figure 1. The figure shows the deployment example of 4 UEs, deployed in the coverage region of 4 HeNBs. The HeNBs are performing CoMP on distinct component carrier in order to serve the UE1 with higher throughput. So, UE1 is served by 4 component carriers while UE2, UE3 and UE4 are served by a single component carrier. For large uncoordinated campuses of home base stations, the resource split between the campus and neighboring macro base stations as well as the resource usage within the campus of base stations should be optimized. Roughly speaking, using too many resources within the campus may cause resource shortage in the

macro network and increase the interference. Thus, it reduces the expected QoS in the campus as well as the macro network and complicates resource management.

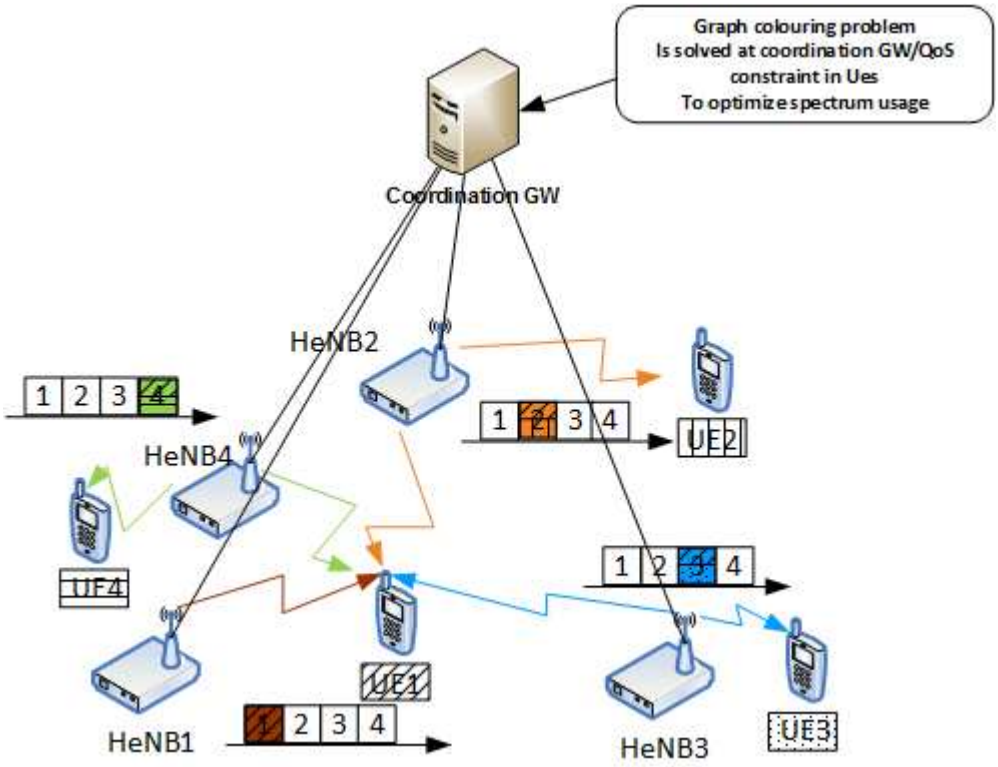

Figure 1: Coordinated carrier aggregation description

2.1.1.1 Graph based techniques for coordinated carrier aggregation

For these reasons, i.e. optimization of the component carriers usage along with throughput improvement, we propose graph coloring based CCA. The basic steps of the graph based coordinated carrier aggregation are given as:

1. Construction of the interference graph at the coordination GW based on the active users measurements and/or combined with neighboring relation tables stored in the base stations of the campus.

2. Coordination GW performs node coloring of the interference graph in order to determine the minimum amount of disjoint component carriers needed to perform the coordinated carrier aggregation for the user terminals in the coverage of the campus of the home base stations.

3. Resource marking and allocation is performed by the coordination GW based on the current distribution of active users in the campus in order to ensure coordinated transmission to the users based on the available component carriers in the network.

Initial simulation results are shown to illustrate the performance of the coordinated carrier aggregation both in terms of componet carrier usage and throughput for different deployement configurations.

2.1.1.2 Interference graph construction

Coordinated multipoint transmission is coordinated transmission for a user terminal of multiple streams from neighboring base stations. The principle is to transform the interference signals into useful signals for the user terminal in order to improve its throughput in the coverage region of the campus. In order to obtain the maximum throughput improvement for the maximum number of user terminals, each UE is needed to set coordinated multipoint with the most interfering base station of the campus among neighboring base stations of its serving base station.

This basic idea of the interference graph construction of the campus is as follows :

- Each node of the graph represent one HeNB of the campus.
- Two nodes (i) and (j) are linked by an edge if HeNB (j) is the most interfering base station for at least one user terminal attached to the HeNB (i).

Other construction metrics are also possible. For example, one can link nodes (i) and (j) by an edge if HeNB (j) is the most interfering base station for a majority of the user terminals attached to the HeNB (i) or for an average of user terminals of the HeNB (i).

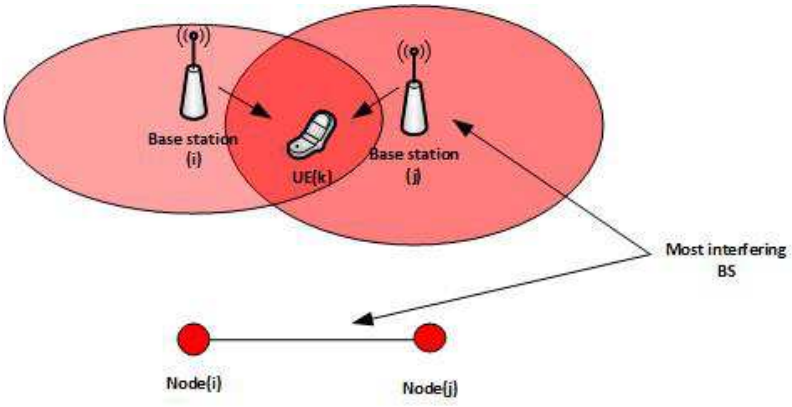

Figure 2: Interference graph construction idea

We have plotted in Figure 2 example of the coverage of the campus of home base stations and the corresponding interference graph. We have used the first metric in the construction, i.e. the most interfering base station for at least one user terminal.

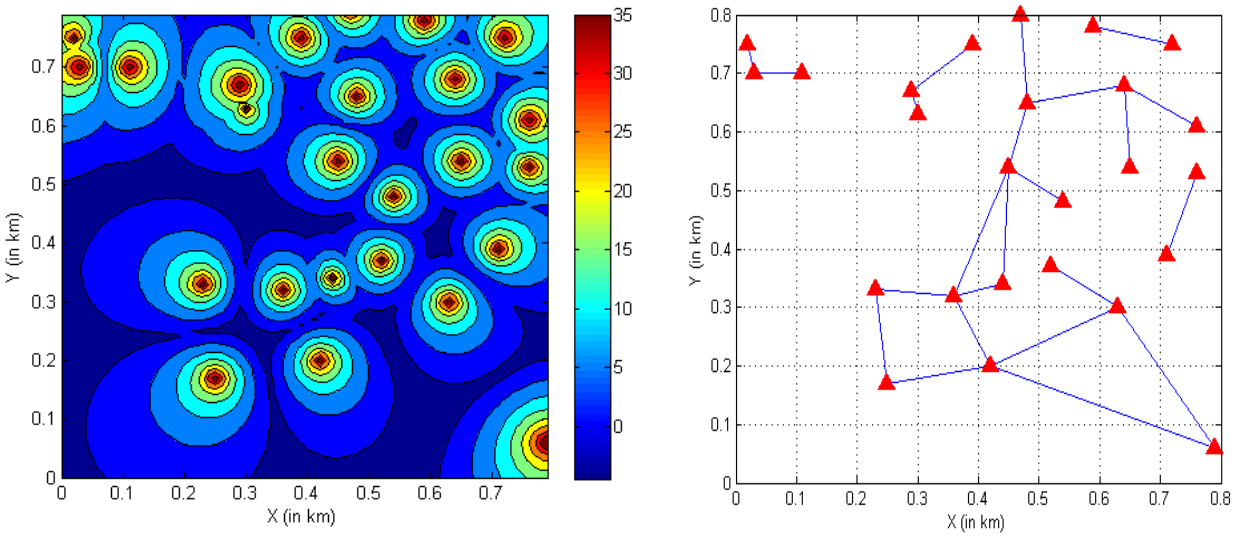

(a) Coverage map of home BS campus coverage

(b) Corresponding interference graph

Figure 3: Coverage and interference graph for typical home base station campus scenario

2.1.1.3 Node coloring algorithms for interference graphs

Node coloring problem consists of choosing from a set of available colors, the *minimal* subset of colors assigned to the nodes of the interference graphs such as two neighboring nodes in the interference graph are colored with distinct colors.

The colors in our contribution denote indices associated to the component carriers needed for coordinated carrier aggregation in the campus for at least one user terminal. In order to achieve the best possible performance for the coordinated carrier aggregation, the neighboring base station should use different resources from the base station the user terminal is currently connected to. So, finding the minimum number resources in order to provide user terminal capable of carrier aggregation, different and non interfering resources is essentially a vertex coloring problem over the interference graph of the campus, i .e. finding the minimum set of colors such that two neighboring nodes of the interference graph are not colored with the same color. Vertex coloring problem is known to be non deterministic polynomial time (NP) hard combinatory optimization problem, i.e. no known polynomial time solution algorithm with linear complexity in the number of nodes for general graph topologies. Various heuristic methods provide coloring that is close to the optimal.

In the next sections, we discuss two popular graph coloring heuristic algorithms and discuss their performance in the context of coordinated carrier aggregation.

2.1.1.4 Largest first ordering sequential node coloring algorithms

The node coloring algorithms proposed in this contribution are based on sequential greedy graph coloring [WEST01], especially on the Welsh-Powell coloring algorithm [WELSH67]. In the sequential greedy coloring framework, the coloring algorithm calculates ordering heuristic and chooses for each node iteratively the *minimum color* not used by its neighboring nodes in the interference graph. Largest first ordering (LF) orders the vertices of the interference graph as a decreasing function of their neighbors, i.e. (degrees of the interference graph). The intuition behind this ordering is to color first the nodes with the higher conflict possibility first. Conflict is defined as reusing the same color by the neighbor of a given colored node. Figure 4 shows an example of largest first sequential graph coloring and the corresponding SINR coverage map for a campus of 25 home base stations and a coverage region of 800x800m that don't take into account the macro base stations interference. We will take into account the macro interference in future work.

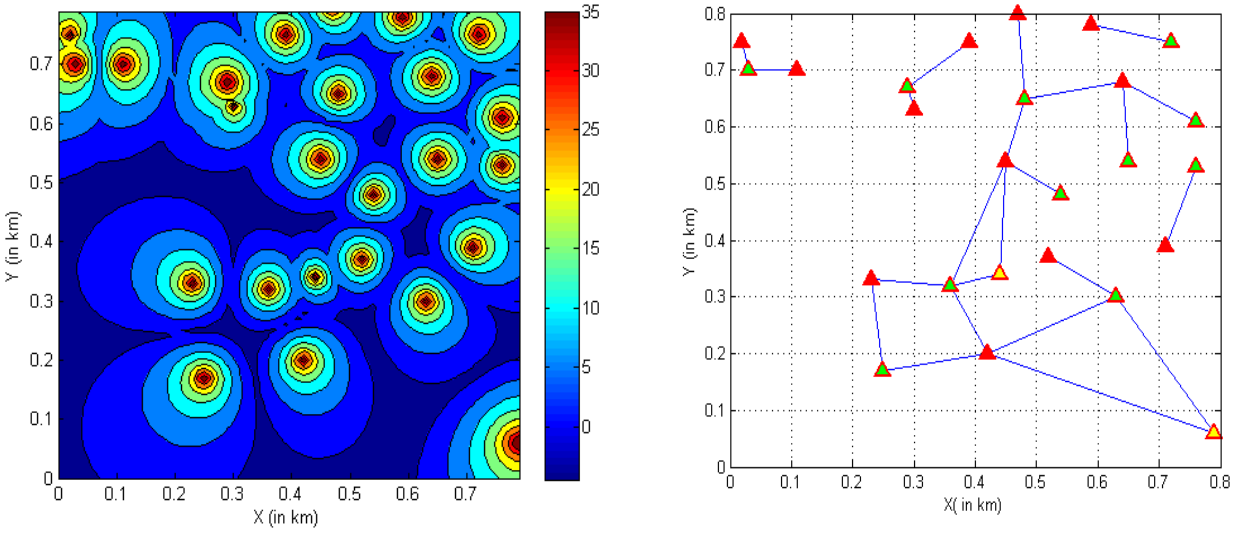

Figure 4: Largest first sequential vertex coloring and corresponding campus coverage

From the figure it is clearly seen that the interference graph is colored with 3 component carriers (CCs) that we will denote *colors* with no conflict, i.e. neigbhouring nodes in the interference graph don't use the same component carrier for serving the carrier aggregation capable users. The Figure 5 illustrates the histogram of the maximum colors needed to color the interference graph with largest first heuristic with the maximum colors reuse CDF.

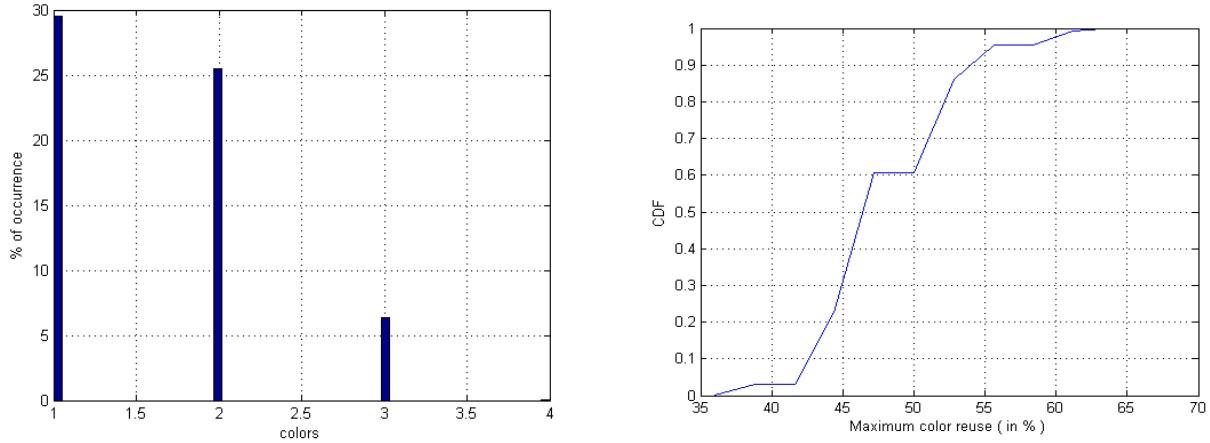

(a) **(b)**

Figure 5: Maximum colors and color reuse CDF averaged over 1000 realizationsof the interference graph

The figure above is showing that the interference graph is colored with 4 colors at maximum for 1% of the campus deployment topologies. The average number of colors needed for providing CCA functionality to the campus is around 1 color. The results we show in Figure 5 were provided for 1000 randomly generated positions of the home base stations and overall traffic density of 50 user terminals in the campus coverage. The average color reuse is evaluated as 50% meaning that at maximum 12 base stations are colored with the same color but different from the colors of their level 1 neighbors.

The performance of the coordinated carrier aggregation CoMP was evaluated next, through system level simulations with two basic assumptions:

1. Serving base stations and neighboring base stations with different color in the interference graph forms coordinated multipoint sets for the user terminals of the serving base stations.
2. The base stations of the campus using similar color that is used by the serving base station contribute to the downlink interference of the serving base station.

In order to evaluate the impact of graph coloring technique over the performance of the coordinated multipoint, we have compared the performance of the GC based CCA system with the scenario where HeNBs are using the same component carrier for CCA. We have also assumed in the simulations that the bandwidth of each home base station is 10MHz.

In Figure 6, initial throughput CDF results are shown for nominal system performance, coordinated CoMP without carrier aggregation and coordinated CoMP with largest first graph coloring.

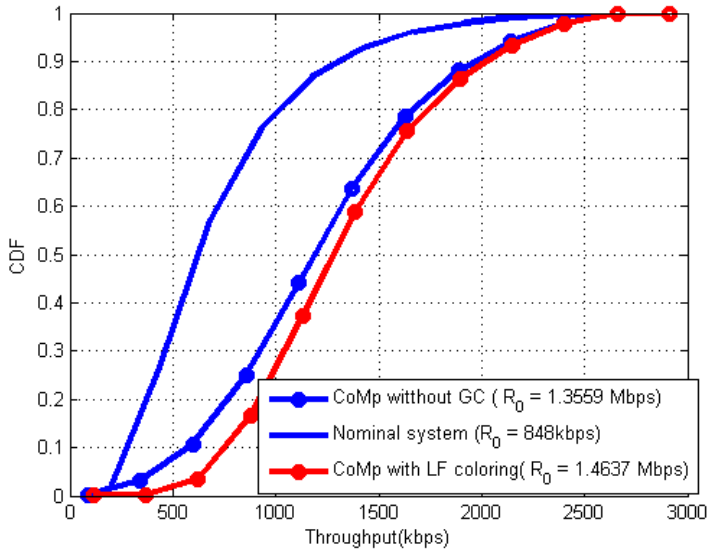

Figure 6: Initial throughput CDF of coordinated carrier aggregation with largest first graph coloring

The simulations of the Figure 6 are performed for a density of 25 home base stations in the campus coverage with average load of 30% of the base stations in the campus. Results are showing that for this campus configuration, the average throughput for the nominal system is R0=848 kbps. Coordinated multipoint transmission without graph coloring, i.e. system that is using unique carrier for CoMP transmission in the campus is showing an average throughput of 1.36 Mbps, which is already an improvement of 60% over the nominal system. The main assumption for throughput calculations in these two cases is standard LTE assumption, i.e. round robin scheduling with physical resource block PRB bandwidth of 180kHz and 50 PRBs per home base station.The average throughput of coordinated multipoint transmission with carrier aggregation and largest first sequential graph coloring is 1.47 Mbps. This performance improves the performance of CoMP of 8% and the nominal system of 73%.

The Figure 7 shows the evolution of the average throughput as function of the average load for the nominal system, CoMP without GC and coordinated CoMP with largest first sequential graph coloring algorithm.

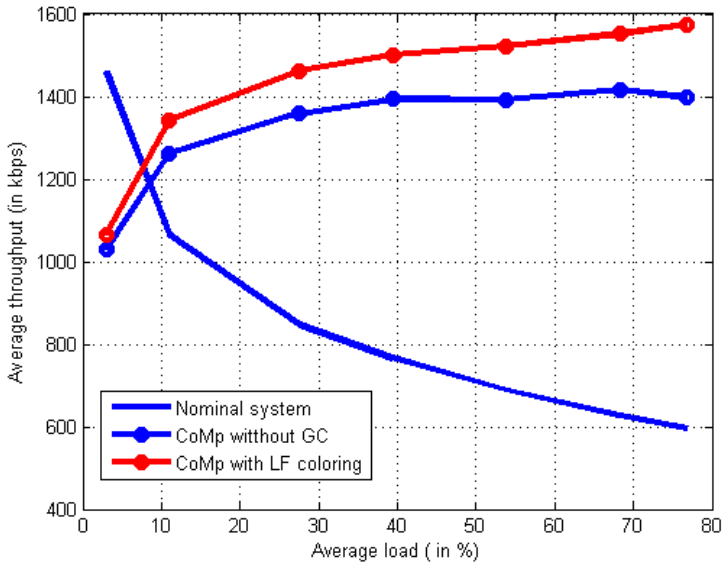

Figure 7: Evolution of the average throughput as function of the base stations load

The results are showing that for low average load, the throughput of the CoMP systems is worse than the performance of the nominal system. This is because CoMP set is constructed from the interference graph derived from measurements of active user terminals. For low load of the home base stations, there is low density of active terminals so the interference graph constructed from these measurements doesn't reflect accurately the interference situation. Solutions will be investigated to solve this problem in future work, among which we may construct interference graph from the measurements of home base stations or from averaging of different graph topologies over longer periods of time.

2.1.1.5 Smallest last ordering sequential node coloring

Smallest last ordering is another important ordering that is proved to be the best ordering for node coloring of planar graphs [KOS03]. Smallest last ordering consists of recursively identifying nodes with the lowest degree in the interference graph and coloring this node as late as possible, i.e. this node is set in the last position of the ordering vector. The Figure 8 shows an example of smallest last sequential graph coloring and the corresponding SINR coverage map for a campus of 25 home base stations and a coverage region of 800x800m.

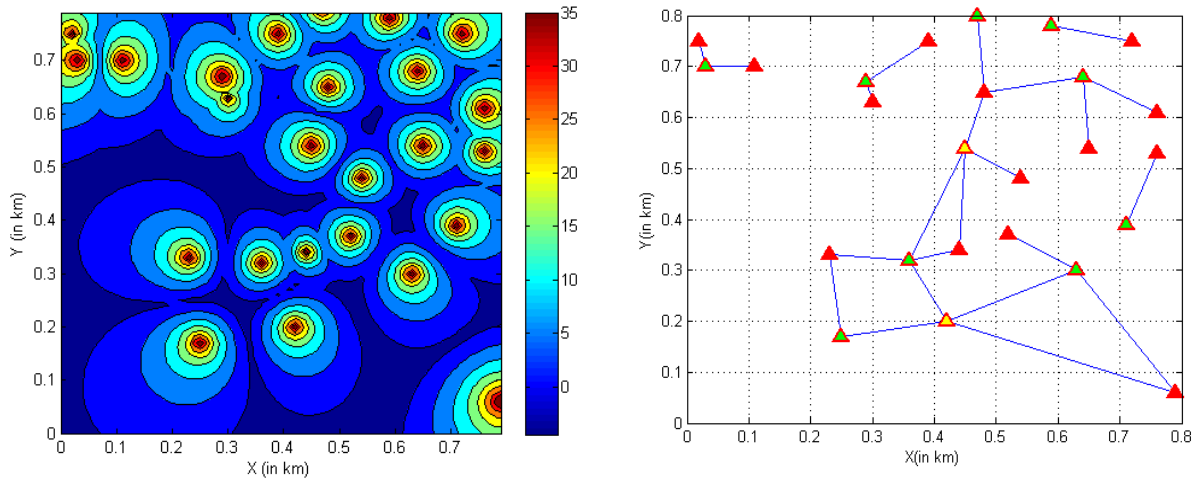

Figure 8: Smallest last sequential coloring example and the corresponding campus coverage

It is seen in this case that the graph is colored with 3 colors as for the largest first coloring example that was shown in Figure 4. In Figure 9 we have shown the histogram of the maximum number of colors needed to color 1000 different topologies of the campus, obtained by randomly generated base stations positions in the campus coverage region. This histogram is provided with the maximum color reuse CDF for smallest last and largest first coloring heuristics.

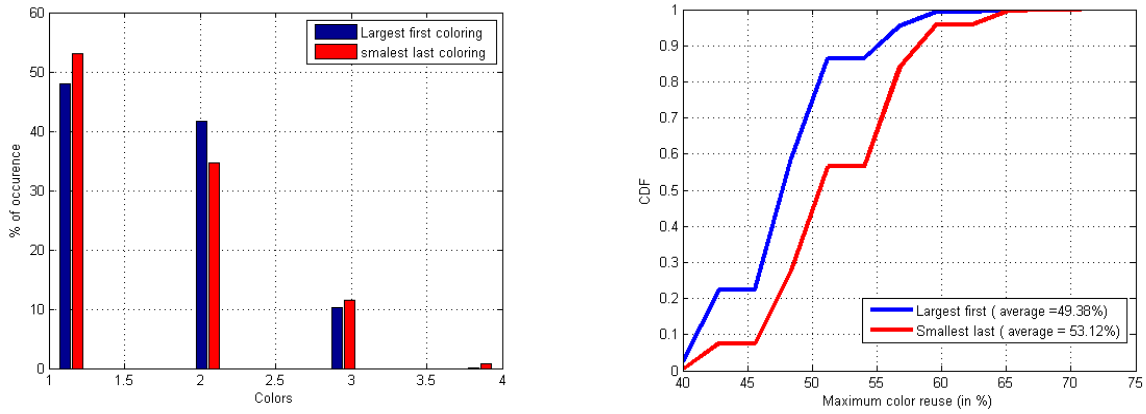

Figure 9: Smallest last sequential coloring compared to largest first coloring (colors and maximum reuse)

Figure above is showing that the smallest last based coloring is reusing more colors than largest first graph coloring. The overall number of colors needed to color the interference graph for the different tested topologies is at maximum 4 colors, i.e. 4 carriers are needed at max for performing the graph coloring based carrier aggregation. The Figure 10 shows the throughput CDFs corresponding to smallest last, largest first based coordinated carrier aggregation and the nominal system, i.e. system without coordinated multipoint.

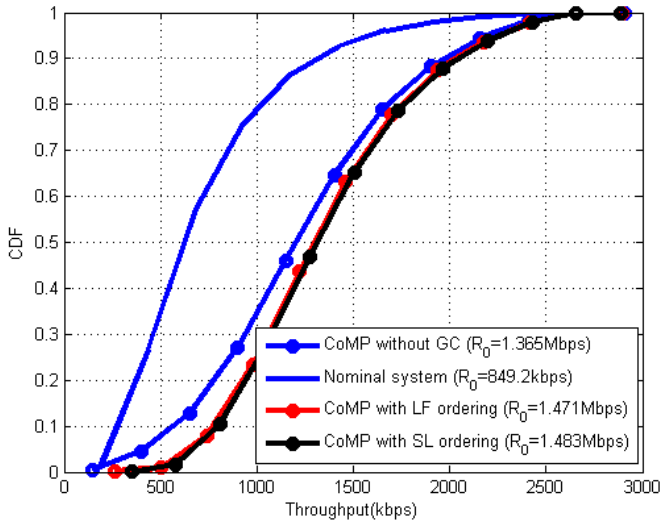

Figure 10: Smallest last sequential coloring performance and comparison with largest first and nominal performance

It is shown in the figure that the average throughput of coordinated CoMP with smallest last sequential graph coloring is around 1.48 Mbps which improves the performance of largest first heuristic of around 1% for the envisioned scenario, i.e. 25 base stations with 30% average load in the campus. Next, the throughput of largest first and smallest last based coordinated graph coloring are compared with the performance of CoMP without graph coloring.

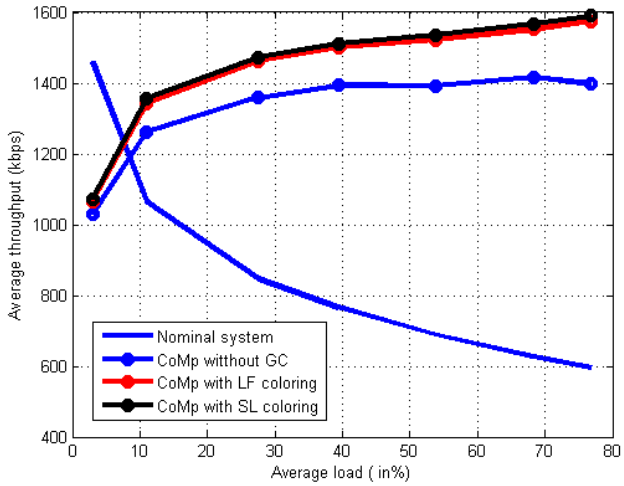

Figure 11: Smallest last sequential coloring performance as function of the loads

The evolution of the throughput of the smallest last based coordinated graph coloring is similar to the throughput of largest first based coordinated carrier aggregation throughput and here also, the improvement of smallest last is at maximum 1%.

2.1.1.6 Conclusion and future work

In this work we have presented an update on graph coloring based carrier aggregation for CoMP in a campus of home base stations scenario, i.e. a group of home base stations that is deployed randomly in the campus coverage area. The overall objective of the study is to

present techniques to provide the optimum reuse of component carriers over the campus while ensuring through CoMP good throughput performance.

The results are showing that at maximum 4 component carriers are necessary for a 25 base stations campus to ensure no interference, i.e. the component carrier of one base station is not reused by the direct neighbors of the base station, so the performance of full interference CoMP can be improved up to 8%. The full interference CoMP system is obtained if we use a unique component carrier for the campus.

We have compared two popular graph coloring heuristics used to implement the coordinated carrier aggregation concept, i.e. largest first ordering and smallest last ordering. The results show that smallest last ordering improves the largest first ordering by 1% in terms of performance and provide the best average component carrier reuse.

Future work will investigate the performance of these two heuristics in very high density scenario and extend the study of CCA for heterogeneous networks of base stations, i.e. network of pico HeNBs relays and including the macro base stations interference in the interference graph calculations.

2.1.2 Multiflow carrier aggregation

The single-flow CA technique is a basic CA approach as introduced by 3GPP LTE Release-10. In single-flow CA, the macrocell is the aggressor cell and the picocell is the victim cell. Taking a toy example consisting of 2 Component Carriers (CCs), while a picocell performs CRE to offload the macrocellular network, and to transmit UE data and UE control signaling on CC1 the macrocell causes intercell interference if no e-ICIC techniques are applied. On CC2, the expanded range pico UE (ERPUE) does not receive any data while regular PUEs are served on CC2. A recent feature in 3GPP LTE Release-12, referred to as multiflow CA or inter-site aggregation, enables a better use of resources and improves system capacity, where multiple base stations (from different tiers) simultaneously transmit data to a UE on different CCs. Dual-connectivity or multiflow CA, in which users are served by different layers on different CCs, has recently emerged as a key research challenge in 3GPP LTE Release-12. Besides the multiflow CA technique, another related approach to provide an efficient and flexible network performance improvement is to split the control- and user-plane (C-and U-plane). In the introduced concept, the C-plane is always provided at low frequency band to maintain good connectivity and mobility. On the other hand, the U-plane is provided by both the macrocells and the small cells (deployed at higher frequency bands) for data transfer. Since small cells are not configured with cell-specific signals and channels, they are named as Phantom Cells. The Phantom Cell Concept is introduced, because of the lack of capacity solutions for high-traffic outdoor environments that can also support feasible mobility and connectivity. Thus, the concept of macrocell assisted picocells has been introduced as a capacity solution that offers mobility support while capitalizing on the existing macrocellular network. Hereby, the C-plane of a picocell UE is provided by a macrocell in a lower frequency band and the U-plane is provided by the picocell at higher frequency bands. For a macrocell UE, both the C-plane and U-plane are provided by the serving macrocell in the same way as in a conventional LTE system. However, a network architecture that supports the C/U-plane split, and interworking between the macrocell and the Phantom Cell is still required.

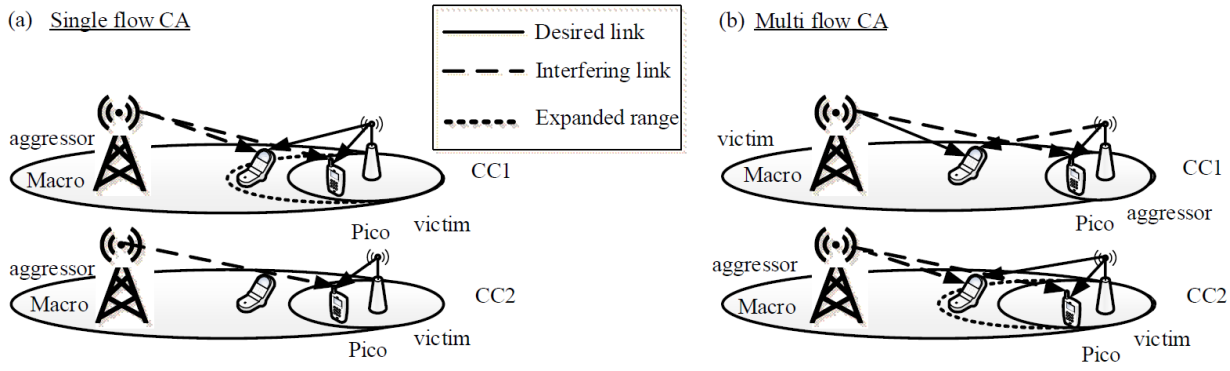

Figure 12: a) Singleflow CA technique b) Multiflow CA technique.

In contrast to the single-flow CA in which the macro base station is always the aggressor cell, in multiflow CA either the macro base station or the pico base station is the aggressor cell. This is because both the macro base station and the pico base station perform CRE on their primary CCs, so that a UE can be served on different CCs by different base stations based on its biased received power. Similar to the single-flow CA learning approach, the multiflow CA based e-ICIC learning algorithm considers the pico base stations and the macro base stations as agents or decision makers. In particular, both the pico base stations and the macro base stations learn their optimal primary CC, CRE bias values and power levels. Algorithm 1 summarizes the steps of the Q-learning based e-ICIC for multiflow transmission. The main difference of the multiflow CA and the single-flow CA based e-ICIC learning algorithm, lies in the action or strategy definition. It is redefined for multiflow CA based e-ICIC as follows:

Action/Strategy per agent: For player pico base station p the action set is defined as $A_p = \{C_p, \beta_p, a_{pr}\} r \in \{1, \dots, R\}$, and for player macro base station m the action set is defined as $A_m = \{C_{mi}, \beta_m, a_{mr}\} r \in \{1, \dots, R\}$, where $C_i i \in \{1,2\}$is the component carrier index that can be selected in order to perform CRE on the selected CC and $\beta \in \{0,6,12\}$ dB is the bias value for CRE on selected CCC_i. Furthermore, a_r is the transmit power level over a set of resource blocks$\{1, \dots, R\}$. Hence, the pico base stations and the macro base stations will independently learn the CCs on which they perform range expansion, with which bias value, and how to optimally perform the power allocation. Since both the pico base stations and the macro base stations can be aggressor cells, different power levels are considered for CCs on which the base stations perform CRE, and the regular CCs which do not have CRE. In addition, the one player formulation case is considered, in which the pico base station is the player. In this case, pico base station carries out the multiflow CA based Q-learning procedure and informs the macro base station about its primary CC and the macro base station uses reduced power levels on this CC and higher power levels on secondary CC of the pico base station. A uniform power allocation is consideredin this case. However, even if no CRE is performed by the macro base station, a UE can be served by both the pico base station and the macro base station on different CCs at the same time based on its biased received power. This learning algorithm will be coined as MF static QL, while the two player algorithm is named MF dynamic QL.

Algorithm 1 Dynamic Q-learning based e-ICIC algorithm for single- and multiflow CA.

loop
  for player p **do**
    Select primary CC $C^p \in \{1, 2\}$
    Select bias value b^p for primary CC C^p
    Select power level a_r^p according to $\arg\min_{a \in \mathcal{A}^p} Q^p(s, a)$ on both CCs
  end for
  Inform player m about primary CC C^p
  for player m **do**
    Select player p's secondary CC as primary CC C^m
    if multiflow CA **then**
      Select bias value b^m for primary CC C^p
    end if
    Select power level $a_r^m \in \mathcal{A}^m$ according to $\arg\min_{a \in \mathcal{A}^m} Q^m(s, a)$
  end for
  Receive an immediate cost c
  Observe the next state s'
  Update the table entry according to equation (1.3)
  $s = s'$
end loop

Figure 13: Proposed Dynamic Q-learning based e-ICIC Algorithm for mutiflow carrier aggregation.

Let us consider a network deployment with multiple picocells overlaying a macro cellular network consisting of 3 sectors per macrocell. A network consisting of a set of $\boldsymbol{M} = \{1, \dots, M\}$ macrocells and a set of $\boldsymbol{P} = \{1, \dots, P\}$ uniformly randomly distributed co-channel picocells per macro sector is considered. We consider that the total bandwidth is divided into subchannels with bandwidth $\Delta f = 180$ kHz. OFDM symbols are grouped into resource blocks (RBs). Both macro- and picocells operate in the same frequency band and have the same number of available RBs, denoted by R. We consider that all transmitters and receivers have single-antennas. A set of UEs $\boldsymbol{U} = \{1, \dots, U\}$ is defined, whereby the UEs are dropped according to scenario #4b[3GPP10a]. We denote by $u(m)$ a macrocell UE, while $u(p)$ refers to a picocell UE. We denote by p_{mr} and p_{pr} the downlink transmit power of macro base station m and pico base station p in RBr, respectively. The SINR at macro UE (MUE) u allocated in RBr of macrocell m is:

$$\gamma_r^{u(m)} = \frac{p_r^{m(u),M} g_{m,u,r}^{MM}}{\underbrace{\sum_{j=1, j \neq m}^{M} p_r^{j(u),M} g_{j,u,r}^{MM}}_{I^M} + \underbrace{\sum_{p=1}^{P} p_r^{m(u),P} g_{p,u,r}^{PM}}_{I^P} + \sigma^2} \quad (1)$$

In eq. **Erreur ! Source du renvoi introuvable.** $g_{m,u,r}^{MM}$ indicates the channel gain between the transmitting macrobase station m and MUE u, $g_{j,u,r}^{MM}$ indicates the link gain between the transmitting macrobase station j and MUE u in the macrocell at base station m, $g_{l,u,r}^{PM}$ indicates the link gain between the transmitting pico base station l and MUE u of macrocell m, and σ^2 is the noise power. Furthermore, I^M and I^P are the interference terms caused by the macro base stations and the pico base stations, respectively.

The SINR at PUE u allocated in RBr of picocell p is:

$$\gamma_r^{u(p)} = \frac{p_r^{p(u),P} g_{p,u,r}^{PP}}{\underbrace{\sum_{j=1,j\neq p}^{P} p_r^{j(u),P} g_{j,u,r}^{PP}}_{I^P} + \underbrace{\sum_{k=1}^{K} p_r^{p(u),M} g_{m,u,r}^{MP}}_{I^M} + \sigma^2} \quad (2)$$

Here, $g_{p,u,r}^{PP}$ indicates the link gain between the transmitting pico base station p and its PUE u, $g_{j,u,r}^{PP}$ indicates the link gain between the transmitting pico base station j and PUE u in the picocell at pico base station p, and $g_{m,u,r}^{MP}$ indicates the link gain between the transmitting macro base station m and PUE u of pico base station p.

The scenario used in the system-level simulations is based on configuration #4b[3GPP10a], and is also defined as scenario 2.7.4 in [D.2.2].

2.1.2.1 Numerical Results

We consider a macrocell consisting of three sectors and $P = \{2,4,8\}$ pico base stations per macro sector, uniformly randomly distributed within the macro cellular environment.

$N_{UE} = 30$ mobile users are generated within each macro sector from which $N_{hotspot} = \lceil 2/3 \cdot N_{UE}/P \rceil$ are randomly and uniformly dropped within a 40 m radius of each pico base station. The remaining UEs are uniformly distributed within the macro cellular area. All UEs have an average speed of 3 km/h. A full buffer model is assumed for the traffic of users. As an evaluation metric, the average UE throughput is considered which is defined as the ratio of number of information bits that the user successfully receives divided by the total simulation time T. If UE u has V downlink packet calls with $W_{v,u}$ packets for the v-th downlink packet call and $b_{w,v,u}$ bits for the w-th packet, the average UE throughput for UE u is:

$$R_u = \frac{\sum_{v=1}^{V} \sum_{w}^{W_{v,u}} b_{w,v,u}}{T} \quad (3)$$

For the proposed frequency domain e-ICIC algorithms an analysis of the tradeoffs for single-flow CA (SF QL) and multiflow CA (MF static QL and MF dynamic QL) is performed. Figure 12 plots the UE throughput for two active picocells per macrocells. While the SF QL and MF static QL algorithms are in average very close to each other, the MF dynamic QL algorithm shows a performance improvement of 47% on average. A close-up view of the cell-edge UE throughput shows that the multiflow CA algorithms outperform the single-flow case. This is because in multiflow CA, cell-edge UEs are served by macro and picocell at the same time. The behavior of the learning based frequency domain e-ICIC algorithms when increasing the number of picocells per macrocell is depicted in Figure 13. Here, the solid curves belong to the left ordinate showing the total throughput and the dashed curves refer to the right ordinate reflecting the cell-edge UE throughput. It can be observed that the MF dynamic QL algorithm outperforms the other algorithms in terms of total throughput while the SF QL algorithm is slightly better than the MF static QL algorithm for less number of picocells (and vice versa for large numbers). The SF QL algorithm shows the lowest performance forcell-edge UE throughput. It can be concluded that cell-edge UEs benefit more from multiflow CA than from single-flow CA. Interestingly, it can be observed that the MF static QL algorithm outperforms the MF dynamic QL for larger number of picocells. This is because in the two-player case, the macro base station cannot fully adapt to the ICIC strategies of all pico base stations in the system, when the number of pico base stations is large. In Figure 14 the sum-rate of the proposed frequency domain e-ICIC algorithms for different number of UEs in case of two picocells per macrocell is depicted.

While the MF dynamic QL algorithm outperforms the other two algorithms, a trade-off between the SF QL and MF static QL algorithm can be seen. For more than 40 UEs per macrocell the MF static QL algorithm outperforms the single flow case. Hence, the multiflow CA technique does not only protect cell-edge UEs, but also improves the total sum-rate at high loads.

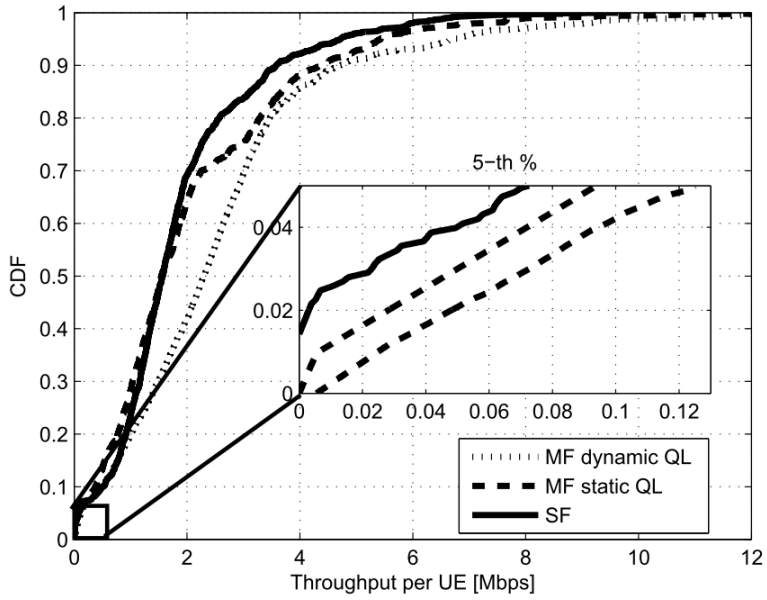

Figure 14: CDF of the UE throughput for the single and multiflow e-ICIC learning algorithm for 2 picocells per macrocell.

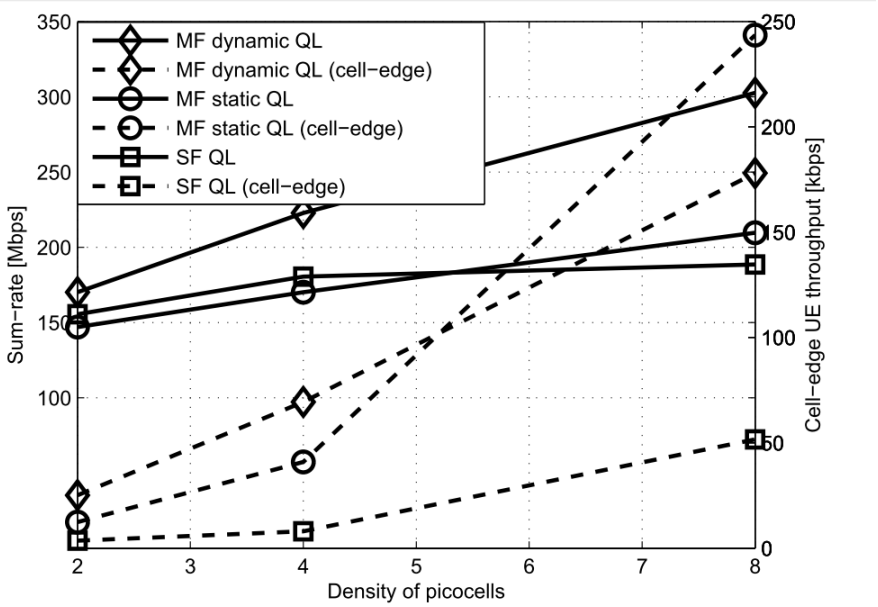

Figure 15: Total-throughput and cell edge throughput versus the number of picocellsin frequency domain e-ICIC.

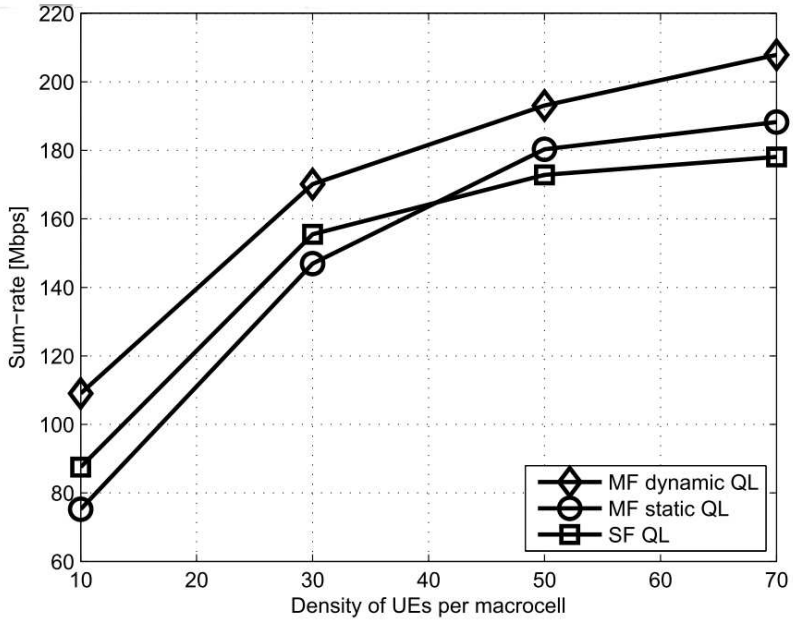

Figure 16: Sum-rate versus the number of UEs per macrocell in the frequency domain.

2.1.2.2 Conclusion and future work

In this work we have investigated the problem of multiflow carrier aggregation in which a given user is served simultaneously by different base stations on different component carriers. This is modelled by means of a dynamic Q-learning formulation in which both macro and picocells learn their optimal cell range expansion bias over different component carrier. Moreover, we have examined the tradoff of single vs. multiflow carrier aggregation as a function of the number of users and deployed cells showing an insight into when to use single and multiflow carrier aggregation. In our future work we will look at the ultra dense network deployment scenario and further extend the multi-flow carrier aggregation to the case of massive MIMO.

2.2 Distributed RRM and synchronization

2.2.1 Distributed RRM (power control) with unpredictable traffic arrival and mobility

The objective of this work is to develop an advanced distributed power control strategy taking into account the dynamic traffic patterns. It is assumed that the traffic arrival has an unpredictable distribution and that the transmit nodes do not exchange information between each other. We consider a wireless network model consisting of multiple transmitters and multiple receivers over an interference channel. All the transmitters and receivers are operating in the same frequency band thereby incurring interference on each other. Let $a_{k,j}(t)$ denote the traffic arriving in the queue of transmitter j at time t and intended to receiver k. Let $x_{k,j}(t)$ denote the data transmitted to receiver k at time t from the queue of transmitter j. The queue update equation for receiver k connected to transmitter j can be written as

$$Q_{k,j}(t+1) = \max\big(Q_{k,j}(t) - x_{k,j}(t), 0\big) + a_{k,j}(t), \forall k, j \tag{4}$$

The service delay of each user (and queue backlog) depends on the deviation between the arrival and the departure rates i.e. $\Delta_{k,j} = \big\|a_{k,j}(t) - x_{k,j}(t)\big\|$. Our objective here is therefore to minimize the quantity $\Delta_{k,j}$ over a finite time horizon T (the connection duration is finite). Minimizing $\Delta_{k,j}, \forall k, j$ over finite time horizon T (especially for small T) is stronger than ensuring the queue stability when $T \to \infty$. Minimizing $\Delta_{k,j}$ over finite T is challenging since the

probability distribution functions of arrival and departure rates are unpredictable (due to for example mobility and interference).

In order to achieve the aforementioned objectives, and make the power control as simple as possible, we model in [MAL13] the evolution of the SINR (in dB scale) as well as the power variation from one timeslot to another as linear dynamic equations. We then formulate an H infinity (H^{∞}) control problem with linear state space equations and quadratic cost. The H infinity framework is a robust solution in the sense that it minimizes the growth of the aforementioned quadratic cost with respect to the norm of the noise whatever the noise. Here, we explain briefly the solution developed in [MAL13].

We artificially introduce a new auxiliary variable denoted by $\gamma^*_{k,n}(t)$. This variable is controlled by our proposed controller. Our objective is then to develop a control strategy such that,

- instantaneous SINR $\gamma_{k,j}(t)$ tracks $\gamma^*_{k,n}(t)$
- $\gamma^*_{k,n}(t)$ tracks the traffic arrival rates
- $\gamma^*_{k,n}(t)$ is feasible at time t.

As a first step in our modeling and to track the feasible values of the target $\gamma^*_{k,n}(t)$ we update it as,

$$\bar{\gamma}^*_{k,j}(t+1) = \bar{\gamma}^*_{k,j}(t) + \beta_{k,j}\left(\bar{\gamma}_{k,j}(t) - \bar{\gamma}^*_{k,j}(t)\right) \quad (5)$$

Where $\bar{\gamma}^*_{k,n}(t)$ denotes the dB value of $\gamma^*_{k,n}(t)$ (with $\gamma^*_{k,n}(0) = \gamma_{k,j}(0)$) and $\beta_{k,j} > 0$ is a very small step size.

The second step in our modeling is to let $\gamma_{k,j}(t)$ to track $\gamma^*_{k,n}(t)$ through power control. The power control should be as simple as possible in order to be implemented in practice. This can be done as follows [SAY05],

$$\overline{P_{k,j}}(t+1) = \varepsilon_{k,j}\left(\bar{\gamma}^*_{k,j}(t) - \bar{\gamma}_{k,j}(t)\right) + \overline{P_{k,j}}(t) \quad (6)$$

Where $\overline{P_{k,j}}$ is the power in dB scale ($\overline{P_{k,j}}(0) = 0$) and $\varepsilon_{k,j} > 0$ is a small step size between 0 and 1. In [SAY05], the aforementioned power control is used with slight modifications and analyzed in presence of Gaussian disturbances (one can refer to [SAY05] for more details).

The aforementioned power update equation is unstable in stochastic environment with unknown disturbances and does not deal with the average delay requirements of dynamic traffic. Let $\omega 1_{k,j}(t)$ be the disturbance due to SINR temporal variations, after some algebraic manipulations we obtain the following SINR variation equation:

$$\bar{\gamma}_{k,j}(t+1) = \{1 - \varepsilon_{k,j}\}\bar{\gamma}_{k,j}(t) + \varepsilon_{k,j}\bar{\gamma}^*_{k,j}(t) + \omega 1_{k,j}(t) \quad (7)$$

where $\varepsilon_{k,j} > \beta_{k,j}$ is a small step size. A similar update equation of traffic arrivals can be obtained (see [MAL13] for more details). It is worth mentioning that the update equations mentioned above may make the system unstable and will not fullfil our objective. We therefore introduce a control sequence $\mathbf{u}_{k,j}(t) = \begin{bmatrix} u^1_{k,j}(t) & u^2_{k,j}(t) & u^3_{k,j}(t) \end{bmatrix}$. Let $\bar{\gamma}^a_{k,j}(t)$ be the traffic arrival(transformed into a quantity in dB scale) and $\omega 2_{k,j}(t)$ be the traffic variation between times t and $t+1$. We obtain the following update equations in a vectorial form,

$$\mathbf{y}_{k,j}(t+1) = \mathbf{A}_{k,j}\mathbf{y}_{k,j}(t) + \mathbf{B}\mathbf{u}_{k,j}(t)\mathbf{D}\boldsymbol{\omega}_{k,j}(t) \quad (8)$$

Where $\mathbf{y}_{k,j}(t) = [\bar{\gamma}_{k,j}(t) \quad \bar{\gamma}^{*}_{k,j}(t) \quad \bar{\gamma}^{a}_{k,j}(t)]^T$ and$\boldsymbol{\omega}_{k,j}(t) = [\omega 1_{k,j}(t) \quad 0 \quad \omega 2_{k,j}(t)]^T$, $\mathbf{D} = \begin{bmatrix} 1 & 0 & 0 \\ 0 & 0 & 0 \\ 0 & 0 & 1 \end{bmatrix}$ and $\mathbf{A}_{k,j} = \begin{bmatrix} 1-\varepsilon_{k,j} & \varepsilon_{k,j} & 0 \\ \beta_{k,j} & 1-\beta_{k,j} & 0 \\ 0 & 0 & 1 \end{bmatrix}$.

We then seek a control sequence $\{\mathbf{u}_{k,j}\}$ which minimizes the following cost function subject to the above state equation.

$$\min_{u_{k,j}} \max_{\omega_{j,k}} E\left\{\sum_{t=1}^{T}\left(\mathbf{L}^{t}_{k,j}\left(\mathbf{y}_{k,j}, \mathbf{u}_{k,j}\right) - \pi^2 P \boldsymbol{\omega}_{k,j}(t) P^2\right)\right\} \tag{9}$$

where $\boldsymbol{L}^{t}_{k,j}\left(\mathbf{y}_{k,j}, \mathbf{u}_{k,j}\right) = \left\|\mathbf{y}_{k,j}(t)\right\|^2_{Q} + \left\|\mathbf{u}_{k,j}(t)\right\|^2$ and variable π^2 is the level of attenuation. For more details on the above cost function, one can refer to [MAL13][Hinf91].

Using H^{∞} control theory [Hinf91], we then develop to the following robust and distributed power control algorithm,

- Each transmitter allocates its own power using $\overline{P_{k,j}}(t+1) = \varepsilon_{k,j}\left(\bar{\gamma}^{*}_{k,j}(t) - \bar{\gamma}_{k,j}(t)\right) + \overline{P_{k,j}}(t) + u^{1}_{k,j}(t)$
- Each transmitter updates $\bar{\gamma}^{*}_{k,j}$ using $\bar{\gamma}^{*}_{k,j}(t+1) = \bar{\gamma}^{*}_{k,j}(t) + \beta_{k,j}\left(\bar{\gamma}_{k,j}(t) - \bar{\gamma}^{*}_{k,j}(t)\right) + u^{2}_{k,j}(t)$
- Vector $\mathbf{u}_{k,j}(t)$ is updated using $\mathbf{u}_{k,j}(t) = -\mathbf{B}^T \mathbf{M}_{k,j}(t+1)\left(\bar{\mathbf{M}}_{k,j}(t+1)\right)^{-1}\mathbf{A}_{k,j}\mathbf{y}_{k,j}(t)$

Where $\bar{\mathbf{M}}_{k,j}(t+1) = \mathbf{I} + (\mathbf{B}\mathbf{B}^T - \pi^{-2}\mathbf{D}\mathbf{D}^T)\mathbf{M}_{k,j}(t+1)$, $\mathbf{I}$ is the identity matrix and $\mathbf{M}_{k,j}(t) = \mathbf{Q} + \mathbf{A}^T_{k,j}\mathbf{M}_{k,j}(t+1)\left(\bar{\mathbf{M}}_{k,j}(t+1)\right)^{-1}\mathbf{A}_{k,j}$ subject to $\pi^2\mathbf{I} - \mathbf{D}^T\mathbf{M}_{k,j}(t+1)\mathbf{D} > 0 \forall t$ and $\mathbf{M}_{k,j}(T+1) = \mathbf{Q}$. For more details one can refer to [MAL13][Hinf91].

In order to assess the performance of our approach, the mean transmit power consumed by both algorithms is depicted in Figure 17, and the evolved mean queue length is depicted in Figure 18 after 5000 time slots. These results are obtained for 25 transmitter-receiver pairs uniformly distributed in a circular region of radius 500m. The channel is a frequency selective Rayleigh fading channel with exponential delay profile. A Poisson traffic arrival model is considered. The packet size is assumed to be 5 kbits in the simulations. We can see that our algorithm outperforms the opportunistic algorithm developed in [LE06]. The power consumed and the queue length are much less for our algorithm.

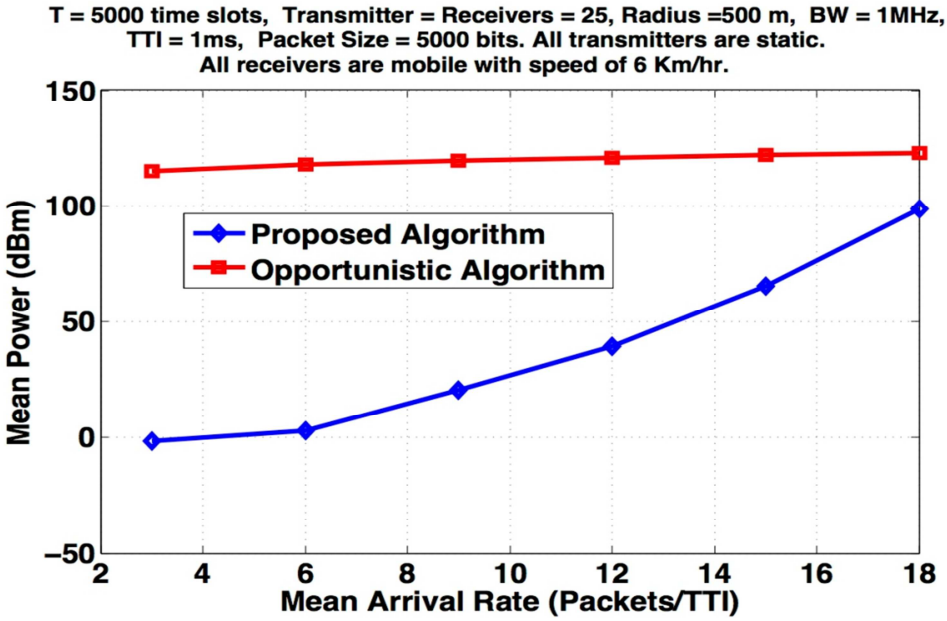

Figure 17: Mean transmit power consumed by the algorithm

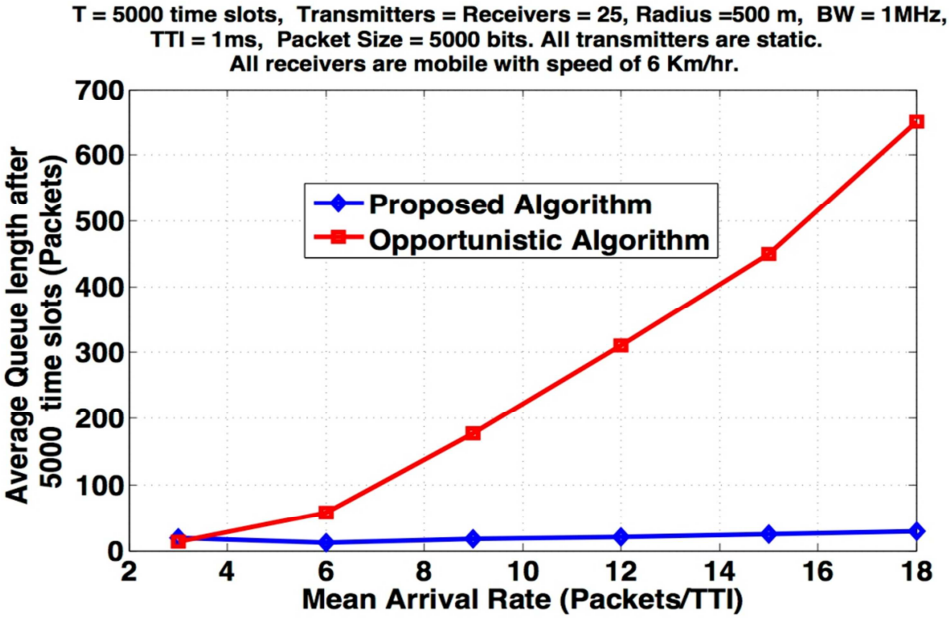

Figure 18: Average Queue length after 5000 packets

This innovation corresponds to scenario 2.9.10 in [D.2.2].

2.2.2 Distributed RRM with no information exchange between transmitters

In this section, we provide a brief description of the work in [MAC13] on distributed RRM with the assumption that the transmitters do not exchange information between each other. Although the framework is general and can be used in many applications, we consider here the context of resource allocation in heterogeneous networks where femto and macro cells co-exist and interfer with each others. Each femto has the objective to minimize its users' SINR outage and in parallel keep its impact on the macro users' outage as small as possible. Notice that here we consider the realistic assumption that, due to mobility and interference, the

transmitters do not have a closed form expression of the SINR density functions. We provide here a fully distributed power control strategy that achieves a Nash equilibrium.

We consider a wireless network comprising two femto cells and one macro cell. We consider a simple setting of one user per cell. The macro access point and the macro user are represented by subscript M and m,respectively, and the femto access point and its user are represented by the subscript F and f, respectively. h_{Mm} represents the channel between the macro access point and the macro user, while $h_{F_j f_i}$ represents the channel between the femto access point j and the femto user i. $h_{F_j m}$ represents the interference channel between the femto access point j and the macro user. Finally, $h_{M f_i}$ represents the channel between the macro access point and the femto user i.

Let $g_{Xx} = |h_{Xx}|^2$ be the channel gain. The downlink SINR of macro user Γ_m is defined as

$$\Gamma_m = \frac{p_M g_{Mm}}{\sigma_m^2 + \sum_{i=1}^{2} p_{F_i} g_{F_i m}} \tag{10}$$

Where σ_m^2 is the noise variance and $\sum_{i=1}^{2} p_{F_i} g_{F_i m}$ represents the interference caused by the femtocells 1 and 2.

The downlink SINR of femto user i, Γ_{f_i}, is defined as

$$\Gamma_{f_i} = \frac{p_{F_i} g_{F_i f_i}}{\sigma_{f_i}^2 + \sum_{j \neq i} p_{F_j} g_{F_j f_i} + p_M g_{M f_i}} \tag{11}$$

Where $\sigma_{f_i}^2$ is the noise variance, $\sum_{j \neq i} p_{F_j} g_{F_j f_i}$ is the inter-femto interference and $p_M g_{M f_i}$ represents the interference coming from the macro access point. In addition, we assume that the macro and femto access points have imperfect knowledge of their own users' SINRs.

We then consider the following problem where the macro user is given priority while maintaining a reasonable quality of service (QoS) for the femto users. Let R_m^k and $R_{f_i}^k$ be the rewards of the macro and the femto respectively. We formulate the following game where macro and femto have the objective to maximize their own reward independently.

$$\begin{aligned} &\max R_m^k = \alpha \boldsymbol{E}_{\gamma_m}[\boldsymbol{P}(\Gamma_m^k \geq \gamma_m)] \\ &\max R_{f_i}^k = \beta \boldsymbol{E}_{\gamma_{f_i}}\left[\boldsymbol{P}\left(\Gamma_{f_i}^k \geq \gamma_{f_i}\right)\right] - \alpha\left(1 - E_{\gamma_m}\left[\boldsymbol{P}\left(\Gamma_{f_i}^k \geq \gamma_{f_i}\right)\right]\right) \end{aligned} \tag{12}$$

Where $\alpha > 0$and $\beta > 0$ are design parameters which can be adjusted to find the desired balance in performance between the femto and the macros. Where $\mathrm{P}(\Gamma_m^k \geq \gamma_m)$ and $\mathrm{P}\left(\Gamma_{f_i}^k \geq \gamma_{f_i}\right)$ are given by,

$$\mathrm{P}\left(\Gamma_{f_i}^k \geq \gamma_{f_i} \middle| D_x^{k-1}\right) = \int_{\gamma_{f_i}}^{\infty} \Phi\left(\Gamma_{f_i}^k \middle| D_x^{k-1}\right) d\Gamma_{f_i}^k \tag{13}$$

$$\mathrm{P}(\Gamma_m^k \geq \gamma_m | D_x^{k-1}) = \int_{\gamma_m}^{\infty} \Phi(\Gamma_m^k | D_x^{k-1})\, d\Gamma_m^k \tag{14}$$

Where D_x^{k-1} is the set of previous SINR measurements till time k-1. To evaluate the above probabilities we need to track the densities of $\Phi\left(\Gamma_{f_i}^k \middle| D_x^{k-1}\right)$. In [MAC13], we provide a distributed bayesian density tracking that allows computing a numerical value of the aforementioned rewards. One can refer to [MAC13][SAL93] for more details.

A solution to the above problem is a state-independent equilibrium in the sense that no node has incentive to change its action when the other nodes keep their choice and the equilibrium strategy does not depend on the state. It may depend on the entire distribution of states. In [MAC13], we develop a distributed algorithm that converges to the Nash equilibrium. Notice that the game here is based only on numerical observation of the rewards (non-model based game). The algorithm is as follows.

At each time instant k, each transmitter updates its power p_X^k, by adding the sine perturbation to the intermediary variable $\hat{p}_X^k$ (using the first equation below), and makes the transmission using p_X^k. Then, each transmitter gets a realization of the reward R_x^{k+1} from its corresponding receiver at time $k+1$ which is used to compute $\hat{p}_X^{k+1}$ using the second equation below.

$$p_X^k = \hat{p}_X^k + a_X \sin\left(\Omega_X \hat{k} + \phi_X\right) \tag{15}$$

$$\hat{p}_X^{k+1} = \hat{p}_X^k + \lambda_k l_X a_X \sin\left(\Omega_X \hat{k} + \varphi_X\right) R_x^k \tag{16}$$

Where a_X and l_X are small step sizes. λ_k is a vanishing step size (e.g. $\lambda_k = \frac{1}{k+1}$). The other parameters are as follows: $\hat{k} := \sum_{k'=1}^{k} \lambda_{k'}$, $\Omega_X \neq \Omega_{X''}, \Omega_{X''} + \Omega_X \neq \Omega_{X'}$ ~~and $\Omega_{X''} \forall i$ are small (e.g.),~~ and $\phi_X \in [0,2\pi]\ \forall X \in \{M, F_1, F_2\}$, $k \in Z$.

In [MAC13], we provide numerical results to assess the performance of our framework. The macro cell radius is equal to 500m whereas the coverage radius of each femtocell is 25m. We consider a frequency selective Rayleigh fading channel with exponential delay profile. The power spectral density of noise is -174 dBm/Hz. We compare our framework to the standard power control scheme [YAT95].Figure 19 **Erreur ! Source du renvoi introuvable.** shows that with our proposed scheme, femto and macro cells are able to maintain a success probability of 65 – 75% which is much better than the standard power control method [YAT95]. Figure 20 ~~**Erreur ! Source du renvoi introuvable.**~~ shows the Pareto boundary for our setting generated by using all possible transmit power scenarios by all the access points. The ellipse in this figure represents our operating region which is quite close to the boundary.

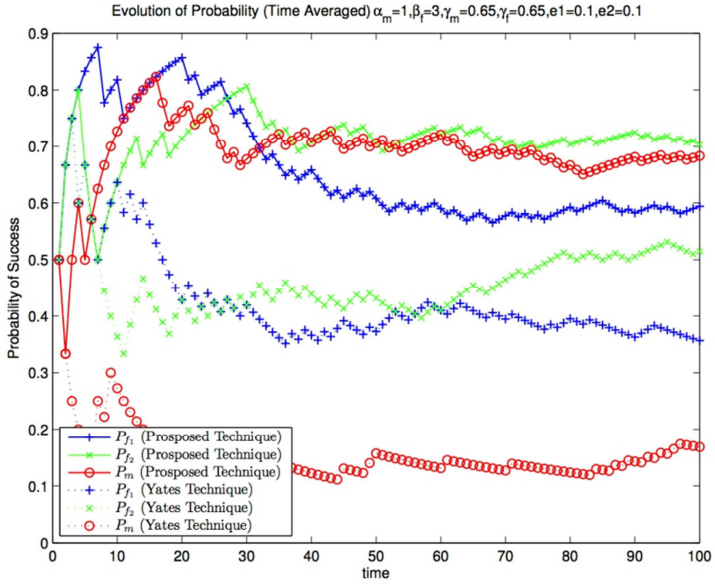

Figure 19: Evolution of success probability

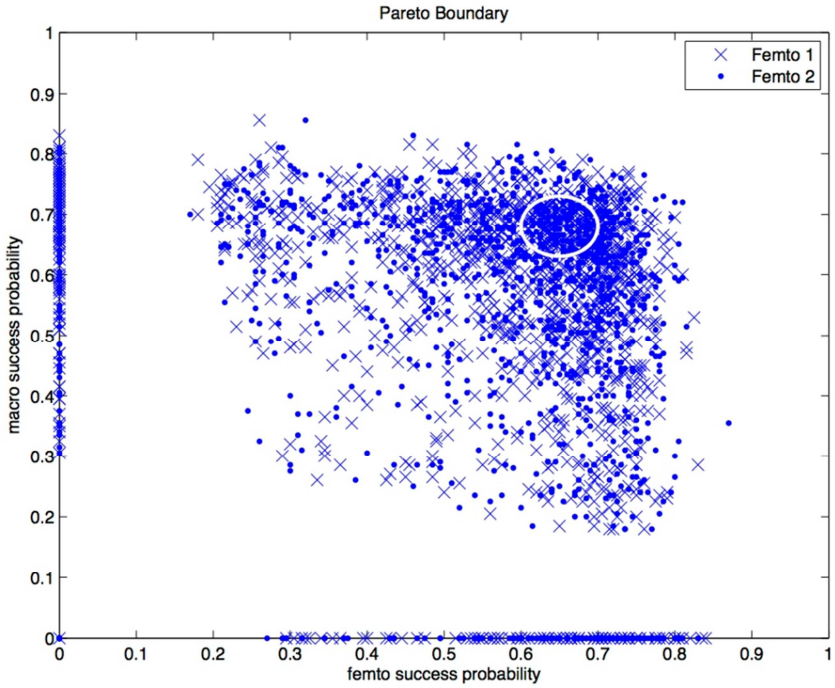

Figure 20: Pareto boundary

This innovation corresponds to scenario 2.9.10 in [D.2.2].

2.2.3 Distributed synchronization algorithm based on over-the-air signalling transmission for heterogeneous network deployments

An inter-node time and frequency synchronization is a strong requirement for enabling cooperation at the physical layer of wireless communication systems. Indeed, CoMP transmission or coordinated scheduling for interference mitigation cannot provide their promised gain under time synchronization mismatch of few micro seconds. The goal of our contribution is to provide efficient inter-node synchronization techniques.

In heterogeneous networks with random and dense deployments of small cells (pico, femto, relays), the core network architecture is in general not related to the wireless network connectivity. Thus, it is preferable to relay on over-the-air synchronization techniques or radio neighbors than using state of art network time protocols that can provide synchronization accuracy between few micro seconds up to few milliseconds according to the network topology. From the physical layer perspective, the target is to achieve a low synchronization error between radio neighbors even if tight synchronization is not achieved globally with respect to a reference clock.

Furthermore, the randomness of the heterogeneous deployments which evolves through time (for example because of nodes on/off) makes it suitable to have a non-coordinated synchronization technique, where each node can adapt to the neighborhood without any master-slave relationship.

Thus, we propose to investigate how consensus algorithms can help in this context, and particularly what would be the impact of nodes imperfect clocks and non-negligible propagation delays, which have not been investigated yet in the consensus literature.

2.2.3.1 Consensus for decentralized synchronization with full duplex nodes

We first consider a wireless mesh network comprising N nodes having full-duplex transmission/reception capabilities. The wireless mesh network connectivity is represented by a graph $\mathcal{G}$, where $\mathbf{C}$ is the $N \times N$ adjacency matrix of the graph. The graph has one connected component, i.e., a path in the graph exists between any two nodes.

We propose a decentralized synchronization algorithm based on timing exchange between nodes at a rate of T unit of time. At each iteration or step n, each node broadcasts a

synchronization sequence at time $t_{k,n} = t_{k,n-1} + T + \varepsilon_k$, where ε_k is a clock drift occurring at the k-th node between two synchronization steps with respect to an absolute perfect reference clock. This clock drift is linked to the quality of the hardware oscillator. The k-th node receives a superimposition of the synchronization sequences from the transmitting neighboring nodes, and can estimate the mis-synchronization with each node by using correlation-based detection techniques. For example, the timing difference observed with node j is $(t_{j,n-1} + T + \varepsilon_j) - (t_{k,n-1} + T + \varepsilon_k) + \tau_{j,k}$, where $\tau_{j,k}$ is the propagation time between the two nodes. Thus, at each step n, the k-th node updates its synchronization time $t_{k,n}$ according to its local clock by doing an averaging of the relative synchronization time received from other nodes, as follows:

$$t_{k,n} = t_{k,n-1} + T + \varepsilon_k + \beta \sum_j \mathbf{C}(k,j)\left(t_{j,n-1} + \varepsilon_j - t_{k,n-1} - \varepsilon_k + \tau_{j,k}\right) \quad (17)$$

where $\mathbf{C}(k,j) = 1$ if the k-th and j-th node are connected, and is null otherwise.

We define $\mathbf{\Phi}_n$ as a vector whose k-th entry is the mis-synchronization $\mathbf{\Phi}_n(k) = t_{k,n} - t_{0,n}$ at step n between the k-th node and an absolute reference clock $t_{0,n} = t_{0,n-1} + T$. From equation (17), the whole system model can be rewritten in a matrix form as

$$\mathbf{\Phi}_n = (\mathbf{I} - \beta\mathbf{L})(\mathbf{\Phi}_{n-1} + \boldsymbol{\varepsilon}) + \beta\mathcal{D}(\mathbf{C}\boldsymbol{\tau}) \quad (18)$$

where $\mathcal{D}(\mathbf{X})$ creates a vector with the diagonal elements of $\mathbf{X}$. By definition, the matrix $\mathbf{L}$ is the combinatorial Laplacian matrix of the graph, i.e., the subtraction between the diagonal degree and adjacency matrices, which is symmetric and can be diagonalized into

$$\mathbf{L} = \mathbf{\Delta}_{|\mathbf{C}|} - \mathbf{C} = \mathbf{V}\mathbf{\Delta}\mathbf{V}^T \quad (19)$$

where $\mathbf{\Delta}_{|\mathbf{C}|} = diag(|\mathbf{C}_1|, \dots, |\mathbf{C}_N|)$ and $|\mathbf{C}_j| = \sum_{k=1}^{N} \mathbf{C}(j,k)$ is the degree of the j-th node at step n, i.e., the number of neighbors from which it receives a synchronization signal at step n, and $\mathbf{\Delta} = diag(\delta_1, \dots, \delta_N)$. It has to be noted that $\mathbf{1}^T \times \mathbf{L} = \mathbf{0}^T$ and $\mathbf{L} \times \mathbf{1} = \mathbf{0}$. Thus, the Laplacian matrix has one null eigenvalue $\delta_1 = 0$ associated to the eigenvector $\mathbf{1}/\sqrt{N}$. When the graph has one connected component, the other eigenvalues $\delta_i > 0$ are strictly positive.

By solving the recurrence in equation (18), one obtains

$$\mathbf{\Phi}_n = (\mathbf{I} - \beta\mathbf{L})^n\mathbf{\Phi}_0 + \sum_{j=1}^{n} (\mathbf{I} - \beta\mathbf{L})^j\boldsymbol{\varepsilon} + \beta\sum_{j=0}^{n-1} (\mathbf{I} - \beta\mathbf{L})^j\mathcal{D}(\mathbf{C}\boldsymbol{\tau}) \quad (20)$$

where $\mathbf{I} - \beta\mathbf{L}$ is doubly stochastic.

2.2.3.1.1 Analysis of the delay-free and clock drift- free system

In order to ensure a convergence of the system with no delay (i.e., $\boldsymbol{\tau} = 0$) and clock drift (i.e., $\boldsymbol{\varepsilon} = 0$), we focus on $(\mathbf{I} - \beta\mathbf{L})^n = \mathbf{V}(\mathbf{I} - \beta\mathbf{\Delta})^n\mathbf{V}^T$, where one must satisfy

$$\forall i > 2, |1 - \beta\delta_i| < 1 \quad (21)$$

which is for example achieved by setting $0 < \beta < 1/max(|\mathbf{C}_i|) < 2/max(\delta_i)$. The higher the value of β, the higher the convergence speed of the system. As a result, when equation (20) is satisfied, $(\mathbf{I} - \beta\mathbf{\Delta})^n$ asymptotically has only one non-null eigenvalue equal to one, and associated to the null eigenvalue of $\mathbf{L}$ and its eigenvector $\mathbf{1}/\sqrt{N}$. Thus, we obtain the asymptotic expression

$$(\mathbf{I} - \beta\mathbf{\Delta})^n \mathbf{\Phi}_0 \sim \frac{\mathbf{1}\mathbf{1}^T}{N} \mathbf{\Phi}_0 \tag{22}$$

which proves that the system with no propagation delay and clock drift converges to a consensus, and that perfect synchronization is achieved in a decentralized fashion.

2.2.3.1.2 Analysis of the impact of the delay and clock drift on the consensus

Let us first analyze the asymptotic expression of

$$\sum_{j=0}^{n-1} (\mathbf{I} - \beta\mathbf{L})^j = \mathbf{V} \sum_{j=0}^{n-1} (\mathbf{I} - \beta\mathbf{\Delta})^j \mathbf{V}^T = \mathbf{V}\mathbf{\Delta}'\mathbf{V}^T \tag{23}$$

where $\mathbf{\Delta}' = diag(\delta'_1, \cdots, \delta'_N)$. By using $\delta_1 = 0$, we obtain $\delta'_1 = n$. The convergence property (20) being satisfied for the other eigenvalues, we obtain $\forall i > 1$

$$\sum_{j=0}^{n-1} (1 - \beta\delta_i)^j = \frac{1}{\beta\delta_i}[1 - (1 - \beta\delta_i)^n] \sim \frac{1}{\beta\delta_i}$$

The matrix $\beta\mathbf{L} + \frac{\mathbf{1}\mathbf{1}^T}{nN}$ is invertible, and the eigenvalues of $\left(\beta\mathbf{L} + \frac{\mathbf{1}\mathbf{1}^T}{nN}\right)^{-1}$ are $\{n, \frac{1}{\beta\delta_2}, \cdots, \frac{1}{\beta\delta_N}\}$. Thus,

$$\sum_{j=0}^{n-1} (\mathbf{I} - \beta\mathbf{L})^j \sim \left(\beta\mathbf{L} + \frac{\mathbf{1}\mathbf{1}^T}{nN}\right)^{-1} = \frac{(n-1)\mathbf{1}\mathbf{1}^T}{N} + \left(\beta\mathbf{L} + \frac{\mathbf{1}\mathbf{1}^T}{N}\right)^{-1},$$

which finally leads to (by using $1^T\mathbf{L} = \mathbf{0}$

$$\mathbf{\Phi}_n \sim \frac{\mathbf{1}\mathbf{1}^T}{N}\mathbf{\Phi}_0 + \left(\beta\mathbf{L} + \frac{\mathbf{1}\mathbf{1}^T}{N}\right)^{-1} [(\mathbf{I} - \beta\mathbf{L})\boldsymbol{\varepsilon} + \beta\mathcal{D}(\mathbf{C}\boldsymbol{\tau})] + (n-1)\mathbf{1}\left[\frac{\mathbf{1}^T\boldsymbol{\varepsilon}}{N} + \beta\frac{\mathrm{Tr}(\mathbf{C}\boldsymbol{\tau})}{N}\right].$$

We observe from this expression that each node of the system experiences the same clock drift. This clock drift is first composed of the average of the nodes clock drift $\mathbf{1}^T\boldsymbol{\varepsilon}/N$, which shows that the consensus algorithm virtually corrects the oscillators errors in each node, especially if these errors have a zero mean for a large hardware deployment. The resulting clock drift is also a function of the averaged accumulated delays of the links arriving to each node of the graph $\mathrm{Tr}(\mathbf{C}\boldsymbol{\tau})/N$, weighted by β.

By assuming that $\mathbf{1}^T\boldsymbol{\varepsilon}/N$ is very small with respect to $\mathrm{Tr}(\mathbf{C}\boldsymbol{\tau})/N$, we can apply a rule of thumbs in order to get the order of the resulting drift. By considering a maximum coverage of 300m for each node, the maximum delay of the inter-nodes link is $1\mu s$. For dense deployments with in average 10 radio neighbors in the coverage area of each node, we get an accumulated delay of $10\mu s$. This corresponds to a 10 p.p.m. clock drift when the periodicity of the decentralized synchronization process is $1s$, which is acceptable. However, the resulting clock drift depends a lot on the deployment density, the robustness of the synchronization sequences detection, and the periodicity of the inter-node synchronization process. Thus, we intend to provide a solution for correcting the drift in all possible cases as a final output of the SHARING project.

From this direct application of the consensus for decentralized synchronization with clock drift and propagation delays, some points needs to be investigated towards a decentralized and non-coordinated wireless synchronization

- The parameter β is chosen according to the highest node degree in the graph, which must be circulated within the graph. We propose to use a weighted consensus method in order to alleviate this constraint.
- Most of the time, wireless communication devices are not full-duplex. It is possible to obtain a consensus by using a scheduling of transmissions and reception steps between neighbors, as often proposed in the literature. This scheduling involves an additional level of coordination which is unfortunate. Thus, we propose a random broadcast strategy, without any master-slave relationship between nodes nor any scheduling, and show in section 2.2.3.3 that is achieved the same behavior as the consensus with full-duplex nodes.

2.2.3.2 Weighted consensus for decentralized convergence parameter selection

In this section, we introduce another strategy for the choice of the correction factors $\boldsymbol{\beta}$. Instead of applying a global correction factor β as in the previous section, we compute the average timing difference of transmitting nodes, i.e. we choose

$$\mathbf{L} = \mathbf{I} - \boldsymbol{\Delta}_{|\mathbf{C}|}^{-1}\mathbf{C} \tag{24}$$

and this leads to

$$(\mathbf{I} - \beta\mathbf{L})^n = (\mathbf{I} - \beta(\mathbf{I} - \boldsymbol{\Delta}_{|\mathbf{C}|}^{-1}\mathbf{C}))^n$$
$$= \boldsymbol{\Delta}_{|\mathbf{C}|}^{-1/2}(\mathbf{I} - \beta(\mathbf{I} - \boldsymbol{\Delta}_{|\mathbf{C}|}^{-1/2}\mathbf{C}\boldsymbol{\Delta}_{|\mathbf{C}|}^{-1/2}))^n\boldsymbol{\Delta}_{|\mathbf{C}|}^{1/2}$$

which behaves as lazy random walk. The matrix $\mathbf{I} - \boldsymbol{\Delta}_{|\mathbf{C}|}^{-1/2}\mathbf{C}\boldsymbol{\Delta}_{|\mathbf{C}|}^{-1/2}$ is known as the normalized Laplacian matrix of the graph and has one null eigenvalue (when the graph has one component) associated to the eigenvector $\boldsymbol{\Delta}_{|\mathbf{C}|}^{1/2}/\sqrt{\mathrm{Tr}(\boldsymbol{\Delta}_{|\mathbf{C}|})}\mathbf{1}$. The other eigenvalues are positive and lower or equal to 2. Thus convergence is guaranteed by choosing $\beta < 2$, and this leads to

$$(\mathbf{I} - \beta\mathbf{L})^n \sim \frac{\mathbf{1}\mathbf{1}^T\boldsymbol{\Delta}_{|\mathbf{C}|}}{\mathrm{Tr}(\boldsymbol{\Delta}_{|\mathbf{C}|})}$$

and we can also show that

$$\sum_{j=0}^{n-1}(\mathbf{I} - \beta\mathbf{L})^j \sim \left(\beta\mathbf{L} + \frac{\mathbf{1}\mathbf{1}^T\boldsymbol{\Delta}_{|\mathbf{C}|}}{n\mathrm{Tr}(\boldsymbol{\Delta}_{|\mathbf{C}|})}\right)^{-1}$$
$$= \frac{(n-1)\mathbf{1}\mathbf{1}^T\boldsymbol{\Delta}_{|\mathbf{C}|}}{\mathrm{Tr}(\boldsymbol{\Delta}_{|\mathbf{C}|})} + \left(\beta\mathbf{L} + \frac{\mathbf{1}\mathbf{1}^T\boldsymbol{\Delta}_{|\mathbf{C}|}}{\mathrm{Tr}(\boldsymbol{\Delta}_{|\mathbf{C}|})}\right)^{-1}.$$

which leads to

$$\boldsymbol{\Phi}_n \sim \frac{\mathbf{1}\mathbf{1}^T\boldsymbol{\Delta}_{|\mathbf{C}|}}{\mathrm{Tr}(\boldsymbol{\Delta}_{|\mathbf{C}|})}\boldsymbol{\Phi}_0 + \left(\beta\mathbf{L} + \frac{\mathbf{1}\mathbf{1}^T\boldsymbol{\Delta}_{|\mathbf{C}|}}{\mathrm{Tr}(\boldsymbol{\Delta}_{|\mathbf{C}|})}\right)^{-1}[(\mathbf{I} - \beta\mathbf{L})\boldsymbol{\varepsilon} + \beta\mathcal{D}(\mathbf{C}\boldsymbol{\tau})]$$
$$+(n-1)\mathbf{1}\left[\frac{\mathbf{1}^T\boldsymbol{\varepsilon}}{N} + \beta\frac{\mathrm{Tr}(\mathbf{C}\boldsymbol{\tau})}{N}\right].$$

where we observe a convergence to the weighted average $\frac{\mathbf{1}\mathbf{1}^T\boldsymbol{\Delta}_{|\mathbf{C}|}}{\mathrm{Tr}(\boldsymbol{\Delta}_{|\mathbf{C}|})}\boldsymbol{\Phi}_0$ when no clock drift or delays are present in the system, and where a common clock drift is observed otherwise.

2.2.3.3 Random broadcast consensus for decentralized synchronization of half duplex nodes

We propose a decentralized synchronization algorithm based on a random broadcast timing exchange, i.e., at each iteration or step n, each node equi-probably selects at random between a transmission or reception state, which leads to the following timing update

$$t_{k,n} = t_{k,n-1} + T + \varepsilon_k + \beta \sum_j \Omega_n(k,j)\big(t_{j,n-1} + \varepsilon_j - t_{k,n-1} - \varepsilon_k + \tau_{j,k}\big), \quad (25)$$

where $\Omega_n(k,j) = 1$ if the k-th is in reception mode and the j-th node is in transmission mode, and is null otherwise.

Let $\mathbf{\Lambda}_n$ be the $N \times 1$ indicator vector of nodes transmitting at step n. If the k-th node is transmitting $\mathbf{\Lambda}_n(k) = 1$, and $\mathbf{\Lambda}_n(k) = 0$ otherwise. The instantaneous connectivity matrix of the directed graph $\mathcal{G}_n$ at step n is denoted $\mathbf{\Omega_n}$ with entries $\Omega_n(k,j)$ and is equal to

$$\mathbf{\Omega_n} = \mathbf{C} * [(\mathbf{1} - \mathbf{\Lambda}_n)\mathbf{\Lambda}_n^T], \quad (26)$$

where $*$ is the element by element matrix multiplication operator and $\mathbf{1}$ is a all-ones vector of length N. Since the nodes choose independently their state one from each other, we obtain that

$$E[(\mathbf{1} - \mathbf{\Lambda}_n)\mathbf{\Lambda}_n^T] = \mathbf{1}\mathbf{1}^T/4 \quad (27)$$

where the division by 4 is the result of the half-duplex property of the nodes. From equation (22), the whole system model can be rewritten in a matrix form as

$$\mathbf{\Phi}_n = (\mathbf{I} - \beta\mathbf{L}_n)(\mathbf{\Phi}_{n-1} + \boldsymbol{\varepsilon}) + \beta\mathcal{D}(\mathbf{\Omega}_n\boldsymbol{\tau}), \quad (28)$$

where the matrix $\mathbf{L}_n$ is the Laplacian matrix of the graph at step n, i.e., the subtraction between the degree and connectivity matrices:

$$\mathbf{L}_n = diag(|\mathbf{\Omega}_{1,n}|, \dots, |\mathbf{\Omega}_{N,n}|) - \mathbf{\Omega}_n,$$

where $|\mathbf{\Omega}_{j,n}| = \sum_{k=1}^{N} \mathbf{\Omega}_n(j,k)$ is the degree of the j-th node at step n, i.e., the number of neighbors from which it receives a synchronization signal at step n.

From (23), (24) and $E\big[|\mathbf{\Omega}_{j,i}|\big] = |\mathbf{C}_i|/4$, we observe that $E[\mathbf{L}_i] = \mathbf{L}/4$ where $\mathbf{L}$ is the Laplacian matrix of the graph $\mathcal{G}$.

The matrices $\mathbf{L}_n$ are i.i.d., which leads to

$$\prod_{i=1}^{n} (\mathbf{I} - \beta\mathbf{L}_i) \sim E[\mathbf{I} - \beta\mathbf{L}_i]^n = (\mathbf{I} - \beta\mathbf{L}/4)^n \quad (asn \to +\infty). \quad (29)$$

and equivalently

$$\textstyle\sum_{j=0}^{n-1} \big(\mathbf{I} - \beta\mathbf{L}_j\big)^j \sim \sum_{j=0}^{n-1} (\mathbf{I} - \beta\mathbf{L}/4)^j$$

Thus, the random broadcast protocol provides the same behavior as the full-duplex algorithms presented in the previous sections with a correction factor 4 on the β factor, which implies a lower convergence speed. This factor 4 comes from the probability $1/4$ to have any two neighbors in the graph transmitting and listening at the same time. Thus, with the

random broadcast protocol, there is no operation scheduling, which involves that the synchronization process is non-coordinated.

2.2.3.4 Simulation results

In this section, we show the initial evaluations of the weighted consensus with random broadcast synchronization method described in this section. We consider a regular LTE tri-sectors eNB deployment illustrated in 0 by the blue circles and a random deployment of small cell. The density of small cells is in average 4 small cells per eNB sector. The system level simulation parameters follows the 3GPP LTE-A requirements. The clock drift of the small cells is 1 p.p.m and the periodicity of the inter-nodes synchronization is 100ms. The inter node propagation delays are computed from the free space propagation model.Figure 22 shows the relative synchronization error between radio neighbors by using a direct synchronization from each small cell to the closest eNB, or by using the proposed distributed synchronization. We observe that the distributed approach improves the inter-nodes synchronization, which takes benefit from cooperation. These first results are encouraging for the next steps we will investigate, as described in next section.

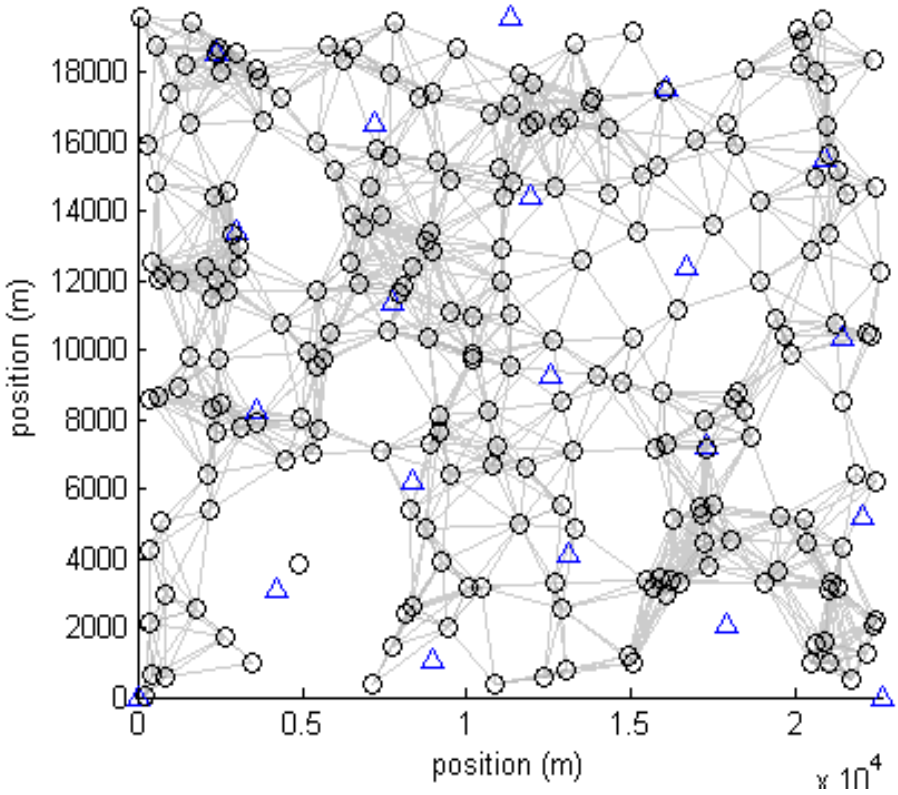

Figure 21: Deployment scenario for outdoor small cells (circles) and eNBs (triangles). The radio links with SNR greater than $-13dB$ are illustrated.

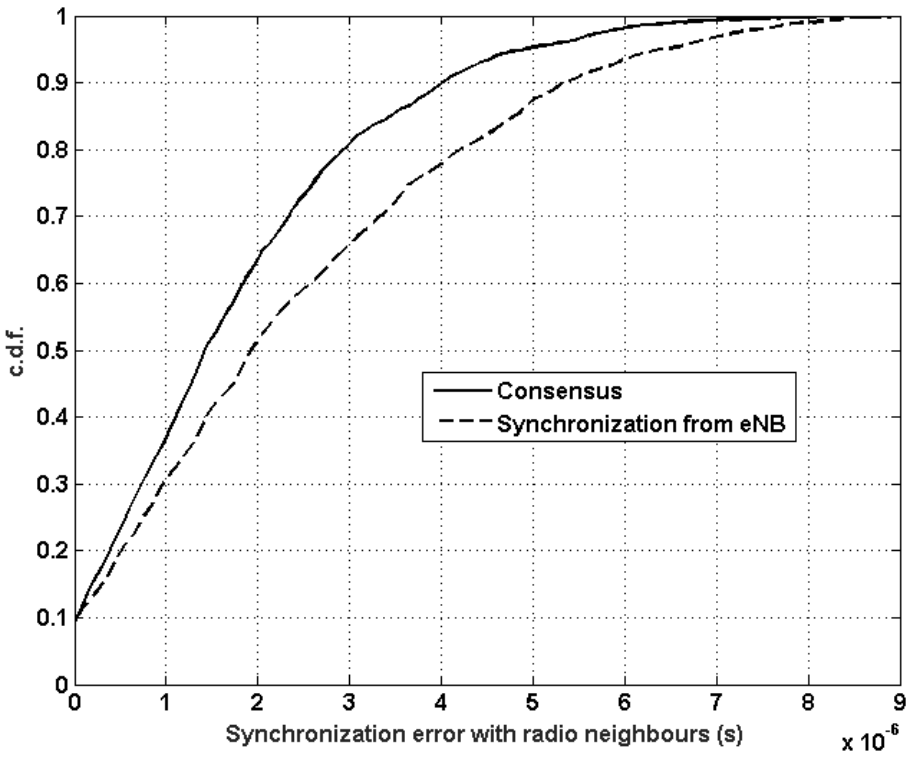

Figure 22: Cumulative density function of the relative synchronization error between radio neighbors.

2.2.3.5 Conclusions and future work

In this section we have presented the main theoretical framework of our contribution for achieving a distributed over the air synchronization between nodes, which is an enabler for several cooperation techniques at the physical layer. We also have made other discoveries that require a more thorough analysis and will be finalized and described in the next deliverable. The next steps of our study are :

- Investigate the possibility to develop a distributed drift correction technique, that will further improve the performance of the distributed synchronization
- Investigate collaboration techniques between layers of the heterogeneous network for the sake of a better inter-node synchronization
- Perform system level simulation according to varying networks densities, scaling, and clock drifts.

3 CONCLUSION

This deliverable has provided an update on the spectrum and resource allocation innovations of task 4.4. The initial concepts were presented in the deliverable [D.4.1]. The main research areas studied in this deliverable are:

- Advanced carrier aggregation techniques for heterogeneous and randomly deployed groups of base stations, presented in section 2.1 of the deliverable.
- Advanced robust decentralized radio resource management with no signaling between the base stations presented in sections 2.2.1 and 2.2.2 of the deliverable.
- Robust decentralized techniques for synchronization and clock drift correction in large groups of femto base stations deployed in the coverage of the macro network layer presented in section 2.2.3.

The overall results are showing that the carrier aggregation related innovations are improving the thoughput of the nominal system by 73% at maximum. Moreover, the studies presented in this deliverable are providing theoretical models of the different carrier aggregation innovations and when to use them.

The decentralized radio resource management sections are presenting models of SON like distributed RRM with low overhead. Results are illustrating that the proposed models effectively optimize the average transmit power and queue lengths and therefore improve both energy efficiency and stability of the network while achieving Pareto bound.

The distributed synchronization section has presented a model of distributed/consensus based synchronization technique that uses the macro base station network to provide fine synchronization to dense network of femto base stations in its neighborhood. It is seen that the proposed random broadcast protocol is improving by around 30% the average synchronization error.

As a prespective, the studies of coordinated carrier aggregation provided in section 2.1.1 are expected to be extended for campuses of heterogeneous networks. Some additional simulation results are expected also for the multiflow carrier aggregation. The results of sections 2.2.1 and 2.2.2 are the final outcome of the decentralized resource allocation studies within the task 4.4 and no future update is expected for these results. The model proposed for distributed synchronization will be further refined and additional system level simulations will be provided for various network densities and considering groups of HeNBs, Picos, …etc. under the coverage of the macro network layer.

REFERENCES

[3GPP10a] 3GPP TR 36.814, v9.0.0 "Evolved Universal Terrestrial Radio Access (E-UTRA); Further advancements for E-UTRA physical layer aspects", March 2010.

[Cis14] Cisco, "Cisco Visual Networking Index: Global Mobile Data Traffic Forecast Update 2013-2018", February 2014.

[D.2.2] Celtic-Plus SHARING, Deliverable D2.2, "Scenarios, KPIs and Evaluation Methodology for Advanced Cellular Systems", 2014.

[D.4.1] Celtic-Plus SHARING, Deliverable D4.1, "New opportunities, challenges and innovative concept candidates for SON/Heterogeneous networks", 2014.

[Eri13] Ericsson, "Ericsson Mobility Report – On the Pulse of the Networked Society", November 2013.

[Hinf91] T. Basar and P. Bernhard, H∞-Optimal *Control and Relaxed Minimax Design Problems: A Dynamic Game Approach.* Birkhauser, Boston, MA, 1991.

[KOS03] Adrian Kosowski, Krystof Manuszewski, "Classical coloring of graphs", available at http://fileadmin.cs.lth.se/cs/Personal/Andrzej_Lingas/k-m.pdf

[LE06] K. K. Leung and C. W. Sung, "An opportunistic power control algorithm for cellular network," *IEEE/ACM Transactions on Networking,* vol. 14, pp. 470-478, Jun. 2006

[MAC13] A. F. Hanif, T. Hamidou, M. Assaad, D. Zeghlache, "Distributed Power Control in Femto Cells using Bayesian Density Tracking", IEEE Allerton conference 2013.

[MAL13] N. Ul Hassan, M. Assaad and H. Tembine, "Robust Power Control in Arbitrary Wireless Networks", IEEE Communication Letters, vol. 17, no 6, pp. 1124-1127, 2013.

[SAL93] N. Gordon, D. Salmond, and A. F. M. Smith, "Novel approach to nonlinear/non-gaussian bayesian state estimation," *Radar and Signal Processing, IEE Proceedings F,* vol. 140, no. 2, pp. 107–113, 1993.

[SAY05] A. Subramanian and A. H. Sayed, "Joint rate and power control algorithms for wireless networks," *IEEE Transactions on Signal Processing,* vol. 53, no. 11, pp. 4204-4214, Nov. 2005.

[WEST01] West D.B. "*Introduction to graph theory"*, Prentice Hall.

[WELSHI67] Welsh D.J.A, Powell M.B, " An upper bound for the chromatic number of a graph and its application to time labeling problems", *The computer Journal* (10),1, pp85-86.

[Yat95] R. Yates, "A framework for uplink power control in cellular radio systems," *Selected Areas in Communications, IEEE Journal on,* vol. 13, no. 7, pp. 1341–1347, 1995.

GLOSSARY

ACRONYM	DEFINITION
3G	Third Generation cellular system
3GPP	Third Generation Partnership Project
ACPR	Adjacent Channel Power Ratio
AM	Amplitude Modulation
ANDSF	Access Network Discovery and Selection Function
AP	Access Point
BLUP	Best Linear Unbiased Prediction
BS	Base Station
BW	Bandwidth
CA	Carrier Aggregation
CAPEX	Capital Expenditure
CC	Component Carrier
CCA	Coordinated Carrier aggregation
CDF	Cumulative Distribution Function
CoMP	Coordinated Multi-Point Transmission and Reception
CRE	Cell Range Extension
CREB	Cell Range Expansion Bias
CRS	Cell-specific Reference Signal
DL	Downlink
eNodeB	Evolved NodeB
GW	Gateway
GC	Graph coloring
HeNB	Home eNodeB
HetNets	Heterogenous Networks
HSPA	High Speed Packet Access
HTTP	Hypertext Transfer Protocol

ID	Identity
ISD	Inter-Site Distance
LF	Largest first vertex coloring
LTE	3GPP Long Term Evolution
LTE-A	LTE-Advanced
MBS	Macro Base Station
MIMO	Multiple-Input Multiple-Output
MUE	Macro UE
NP	Non deterministic polynomial time
OFDM	Orthogonal Frequency Division Multiplexing
OPEX	Operational Expenditure
PRB	Physical Resource Block
PSD	Power Spectral Density
PSNR	Peak Signal to Noise Ratio
PTS	Partial Transmit Sequence
PU	Public
PUE	Pico UE
QL	Q-Learning
QoS	Quality of Service
RB	Resource Block
RE	Range Extension
RL	Reinforcement Learning
RLC	Radio Link Control
RRM	Radio Resource Management
RRU	Remote Radio Unit
RSRP	Reference Signal Received Power
RSS	Received Signal Strength
SBS	Small cell Base Station
SCBS	Small Cell Base Station

SHARING	Self-Organized Heterogeneous Advanced Radio Networks Generation
SINR	Signal to Interference and Noise Ratio
SIR	Signal to Interference Ratio
SNR	Signal to Noise Ratio
SON	Self Optimizing/Organizing Network
SPPP	Spatial Poisson Point Process
UE	User Equipment
UL	Uplink